Distinct sources and behavioral correlates of macaque motor cortical low and high beta

Simon Nougaret[1,*], Laura López-Galdo[1], Emile Caytan[1,2], Julien Poitreau[1,3], Frederic V Barthelemy[4,1], Bjørg Elisabeth Kilavik[1,*]

[1] Institut de Neurosciences de la Timone (INT), UMR 7289, CNRS, Aix-Marseille Université, 13005 Marseille, France

[2] Current address: University of Crete, Faculty of Medicine & Foundation for Research and Technology Hellas, Institute of Applied and Computational Mathematics, Heraklion 70013, Greece

[3] Current address : Laboratoire de Neurosciences Cognitives (LNC), UMR 7291, CNRS, Aix-Marseille Université, Marseille, France

[4] Institute of Neuroscience and Medicine (INM-6), Jülich Research Centre, Jülich, Germany

* Corresponding authors: Simon.Nougaret@univ-amu.fr, Bjorg.Kilavik@univ-amu.fr

HIGHLIGHTS:

- The low beta rhythm is dominant in M1 and the high beta rhythm in PMd
- The beta rhythms correlate with task-instructed and uninstructed behavior
- Low beta reflects movement preparation and spontaneous postural dynamics
- High beta reflects temporal task prediction and dynamical visuospatial attention

BRIEF SUMMARY: Nougaret et al. find that low and high beta rhythms co-reside in the motor cortex. Low beta dominates in M1 and reflects movement preparation but also spontaneous postural changes. High beta dominates in PMd and reflects temporal task prediction but also fluctuations in focal overt attention dedicated to the behavioral task.

Keywords: macaque, local field potentials, motor cortex, beta rhythms, spontaneous movements, postural control, movement preparation, attention, anticipation

SUMMARY

Low and high beta frequency rhythms were observed in the motor cortex, but their respective sources and behavioral correlates remain unknown. We studied local field potentials during pre-cued reaching behavior in macaques. They contained a low beta band (<20Hz) dominant in primary motor cortex and a high beta band (>20Hz) dominant in dorsal premotor cortex. Low beta correlated positively with reaction time from visual cue onset, and negatively with uninstructed hand postural micro-movements throughout the trial. High beta reflected temporal task prediction, with selective modulations before and during cues, which were enhanced in moments of increased focal attention when the gaze was on the work area. This double-dissociation in sources and behavioral correlates of motor cortical low and high beta, with respect to both task-instructed and spontaneous behavior, reconciles the largely disparate roles proposed for the beta rhythm, by suggesting band-specific roles in both movement control and spatio-temporal attention.

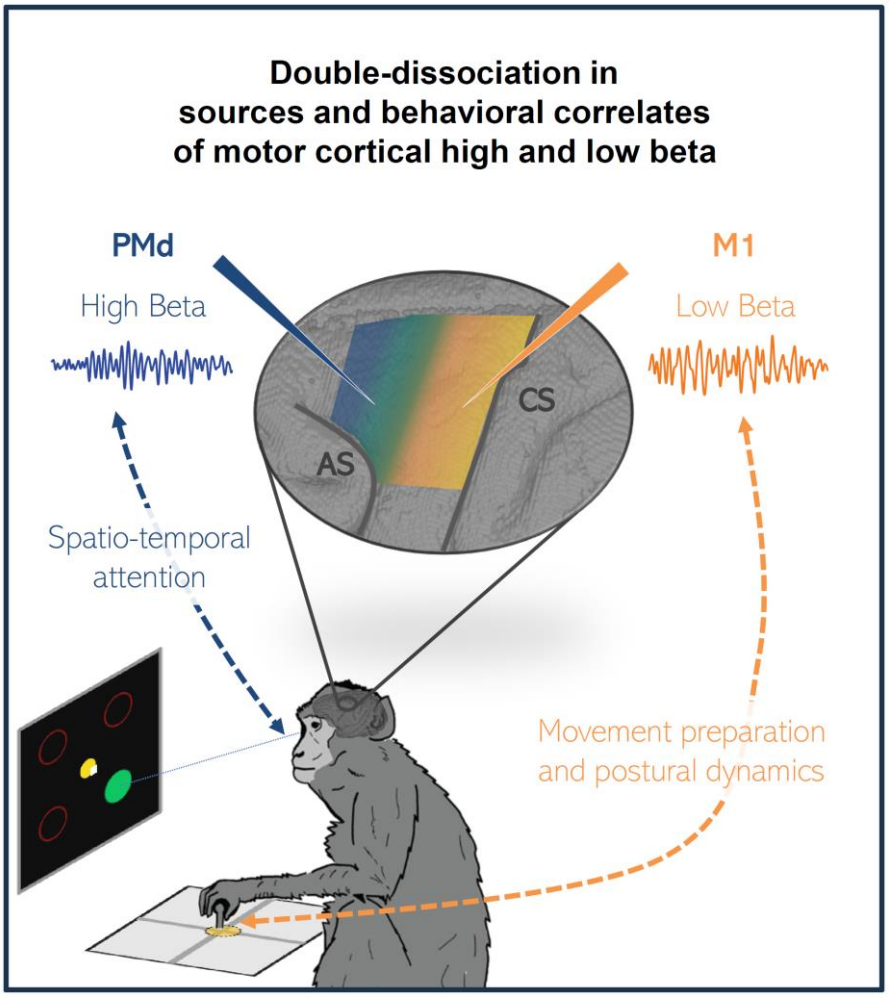

INTRODUCTION

A link between the beta rhythm in human sensorimotor cortex and voluntary movements was established almost 75 years ago[1]. Yet, the functional role of sensorimotor beta remains elusive. Beta was associated with many aspects of motor behavior, ranging from motor cortical idling or postural maintenance[2–11] to sensorimotor integration or temporal predictions[12–22]. As beta rhythms were observed in many cortical and subcortical regions and in many different behavioral contexts, they might serve multiple roles[23–26]

Most studies have treated the broad beta frequency range (~13-35Hz) as one common motor cortical rhythm, possibly rendering the association of specific beta rhythm modulations to specific components of sensorimotor behavior difficult. A few studies divided this broad band into low beta (below 20Hz) and high beta (above 20Hz). In a published dataset[27,28], we observed concurrent and distinct low and high beta bands during visuomotor behavior in macaque motor cortical local field potentials (LFP). However, the low and high bands modulated similarly in power and peak frequency in that behavioral task. Also Stoll et al.[29] observed two distinct low and high beta bands in macaque frontal cortical electrocorticography (ECoG), in a trial-and-error task comprising search and repetition phases. They found only the high band to be systematically sensitive to attentional effort and cognitive control. Chandrasekaran et al.[30] correlated behavioral reaction time (RT) with dorsal premotor cortex (PMd) beta power, in a RT-task. Their data contained a single band peaking at 25Hz, which shifted slightly towards higher peak frequency in the pre-stimulus period for shorter RT, resulting in positive correlations below 20Hz and negative correlations above 20Hz. In comparison, Zhang et al.[31] found positive correlations with RT for sensorimotor pre-stimulus alpha/beta power covering 8-33Hz in a RT task.

These studies remain far from conclusive in determining potentially distinct correlations between behavior and motor cortical low and high beta bands. We therefore designed a new visuomotor behavioral task to maximize at the same time spatio-temporal attention and the required motor control, with the aim of disentangling which of the different task variables, and task-instructed and

uninstructed (spontaneous) behavioral factors[32,33] affect the two beta bands. We hypothesized that low beta might be related to dynamic postural control and movement preparation. This band was shown to be more affected in human Parkinson's disease patients than high beta[34,35], and more attenuated by stimulation in the subthalamic nucleus[36] and levodopa administration[37], two therapies that improve motor control. Furthermore, low beta is attenuated after kinematic errors[38]. In contrast, motor cortical high beta might be more closely associated with attention, working memory, decision-making or reward[29,38–40], and originate anterior to low beta[41]. Consistent with these predictions, we found low beta to be dominant in primary motor cortex (M1) and correlate positively with behavioral RT in two macaques. Low beta also correlated negatively with spontaneous hand postural micro-movements that were frequent during the maintenance of stable central hold during delays. High beta, on the other hand, was dominant in PMd, and was unrelated to RT and hand postural micro-movements. Instead it modulated selectively during anticipation and processing of visual cues. This modulation was enhanced by focal overt attention, when the animal oriented the gaze towards the work area.

RESULTS

We studied LFP low and high beta band rhythms recorded in the motor cortex (M1 and PMd) of two macaque monkeys engaged in a complex visuomotor reaching task. We determined the motor cortical regions in which each band dominated, and we quantified their relationship to task conditions and performance, and to spontaneous hand and eye movements.

Behavioral task performance

Two macaque monkeys performed a delayed match to sample task with fixed cue order and a GO signal, requiring arm reaching responses in one of 4 (diagonal) directions from a common center position. The visuomotor task was complex, requiring the animal to select the valid spatial cue (SC; one out of three sequentially presented SCs; the other two were distractors) that matched in color with a preceding color selection cue (SEL; Fig. 1B). The animal then had to prepare a center-out arm reaching movement to the memorized matching SC position, to be executed after a GO signal. Throughout the sequence of presentation of the different visual cues, the animal had to maintain central hand position with the manipulandum within a very small zone, but was free to explore the visual scene with the eyes.

We analyzed 59 sessions in monkey T and 39 sessions in monkey M. Of all initiated trials, central hand position maintenance was lost before the GO signal in about 40% (Table S1), reflecting the difficulty of initial stabilization and maintenance of the hand manipulandum within the 0.6cm diameter fixation zone. Several types of errors were also made in trials not aborted before the GO signal (GO trials). Of these, directional errors towards a distractor (distractor errors) were in majority (about 20% of GO trials, Table S1). These occurred less frequently when the third and last SC (pink) was valid ($p<0.01$ for both) and somewhat less for movements towards the body (i.e. lower visual field; $p<0.01$ for monkey T, $p=0.036$ for monkey M).

Even if our task entailed an explicit GO signal, dissociated in time from the informative cues, trial–by-trial fluctuations in RT might reflect the level of motor readiness at the time of the GO signal, influenced by movement preparation processes and/or overall level of alertness or fatigue. We

113 quantified the variability in RT across sessions, color conditions and movement directions. All three
114 factors influenced RT, in a similar manner in the two animals ($p<0.01$; Table S1). First, there was a
115 main effect of the session, with different average RT in different sessions, but with no trend of
116 increasing or decreasing RT from early to late sessions. Furthermore, RT was shorter in the pink color
117 condition and for movements towards compared to away from the body.

118 Finally, the RT increased with time-on-task[29,42], being positively correlated with trial number
119 within the session ($p=0.022$ for Monkey T, $P<0.01$ for Monkey M).

120

121 **Spontaneous hand and eye movements**

122 Both animals made spontaneous (uninstructed) movements during the behavioral trial. This
123 included hand micro-movements during the maintenance of the hand cursor within the central
124 fixation spot (Fig. 1C), and gaze shifts to and from the work area (computer monitor), and between
125 the items of the visual scene (Fig. 1D-F). Although uninstructed, these hand and eye movements
126 were aligned to task events and were remarkably similar in the two animals.

127 We used velocity to quantify the hand micro-movements. The trial-averaged hand velocity
128 decreased as the hand stabilized inside the central fixation at trial start, and was minimal at the onset
129 of the valid SC. After valid SC presentation, hand velocity increased, and differed significantly for the
130 three conditions (Fig. 1C and Fig. S1A-C). These micro-movements did not reflect a drift of the hand
131 position in the (diagonal) direction of the upcoming center-out reaching movement (Fig. S1D), unlike
132 the spatial attention effects described for eye fixational microsaccades[43]. Instead, the hand
133 prevalently drifted along one or the other main axes defined by the 2D manipulandum, having lower
134 frictional resistance than for diagonal movements involving both axes. Control electromyographic
135 (EMG) recordings from one of the proximal muscles involved in the task (deltoid) revealed increased
136 muscular tone during the preparatory period following the valid SC onset (Fig. S1E). This increase was
137 similar for preparation of movements towards and away from the body, contrasting with the strong
138 directional selectivity of this muscle during the center-out reaching execution. Thus, the hand micro-

movements during preparation were probably related to increased muscle tone of arm muscles involved in the subsequent reaching movement.

The monkeys frequently made eye movements to explore the items of the visual scene, or to shift the gaze In/Out of the work area (Fig. 1D-F). The gaze was often directed Out, possibly reflecting moments with less focal attention on the task. Monkey M spent more time gazing Out, but less before and during the valid SC and as the GO signal approached. Finally, both monkeys restricted eyeblinks to the delays, thus under tight temporal attention control, as also shown in humans engaged in demanding working memory tasks[44].

Concurrent low beta in M1 and high beta in PMd with distinct amplitude profiles

LFP activity from 110 recording sites (59 sessions) in monkey T and 60 sites (39 sessions) in monkey M was analyzed. Spectrograms for one session with three simultaneously recorded sites (Fig. 2A-C) showed a high beta band (> 20Hz) predominant in the most anterior site (PMd; site 1), and a low beta band (<20Hz) predominant in the most posterior site (M1; site 3). Both bands were distinguishable in the intermediate site (site 2). Even if the trial-averaged spectrograms showed increased beta band power across long periods of the task, single-trial LFPs showed bursts of high beta in PMd (Fig. 2D) and low beta in M1 (Fig. 2F) of variable durations and timing across trials, as already described[13,28,45,46].

Average spectrograms across all trials and LFP sites for each monkey (Fig. 2E) clearly contained a low and a high beta band in both animals, with the low band peaking at 16Hz, and the high band at 26Hz (Fig. 3A). We computed a *beta band dominance index*, after first removing the aperiodic signal component (see Methods), in the delay before SC1 (blue). A small majority of sites had higher power for the low beta band (64/110 sites in monkey T and 38/60 in monkey M; Fig. 3B), the remaining had higher power in the high beta band. We then superimposed the beta band dominance index on the cortical surface reconstruction within the recording chamber. This revealed a gradient with high beta dominant in the anterior recording sites (PMd), and low beta dominant in the posterior (M1) and intermediate sites (Fig. 3C). The band dominance index correlated significantly with antero-posterior

site coordinate within the recording chamber for each animal ($p<0.01$; Spearman's rank order correlation). To confirm local origin of these LFP beta rhythms, we analyzed phase-locking of neurons to the locally dominant beta band, for neurons and LFPs recorded on the same linear array. For the high band dominant sites, 47.7% of neurons (27/60 neurons in monkey T and 45/91 in monkey M) were significantly phase-locked to high beta phase. For the low band dominant sites, 12.3% of neurons (22/269 neurons in monkey T and 38/218 in monkey M) were significantly phase-locked to low beta phase.

Low and high beta peak frequencies (Fig. 3A) and beta band dominance across the cortical surface (Fig. 3C) were similar in the two animals. Since the task performance (Table S1) and spontaneous hand and eye movements (Fig. 1C-F) were also similar in the two monkeys, from hereon we collapsed the data for the two animals. We combined all individual trials from all LFP sites with the same beta band dominance, such that each LFP site was assigned to either contribute to the low or the high band, and the normalized, single-trial instantaneous beta amplitude was calculated (Hilbert transform). The trial-averaged amplitude including all sites from both monkeys differed distinctly for low and high beta (Fig. 4A; Fig. S3A, C). The amplitude of the high band was strong right from the trial start and throughout most trial epochs, only dropping temporarily around each SC. Thus, the high band reflected the 'rhythmic' nature of the sequence of task events. In comparison, the amplitude of the low band increased gradually after trial start and was maximal between SEL and valid SC. It then dropped selectively after the valid cue and remained lower through the remainder of the trial. Both bands had minimal amplitude after GO. Each of the two temporal profiles of average beta amplitude were accompanied by quasi inverse temporal profiles of average local multi-unit activity (MUA) amplitude (Fig. S4). MUA amplitude in high beta dominant sites peaked during valid SC presentation, while MUA amplitude in low beta dominant sites was minimal between SEL and valid SC and elevated during movement preparation. The distinctly different profiles of average MUA amplitude obtained when splitting sites according to beta band dominance add support to an at least partly local origin of the two beta bands.

192 A dimensionality reduction visualization (t-SNE), considering temporal profiles of single-trial
193 amplitude for unambiguous correct trials (i.e. trials with none of the distractors coinciding in space
194 with the valid SC) suggested a larger difference across conditions for the low beta band (insets in Fig.
195 5A). We trained a random forest estimator to decode color conditions based on temporal profiles of
196 either low or high beta amplitude using a subset of unambiguous correct trials. The decoder was
197 tested on the remaining unambiguous correct trials. The decoding performance was significantly
198 above chance level for both bands, but strongest for the low band (Fig. 5B). This strong condition
199 selectivity furthermore prompted us to explore the numerous distractor error trials (see Table S1).
200 Indeed, when the monkey wrongly performed a reach towards one of the distractors, the temporal
201 profiles of low and high beta amplitude reflected the distractor selected by the animal (Fig. 5A). The
202 decoder trained on correct trials could also decode the attended distractor in error trials (Fig. 5C)
203 again with a better accuracy for the low band. In comparison, for both bands the decoder was well
204 below the chance level for decoding the missed valid SC in distractor error trials (Fig. 5C). Thus, both
205 low and high beta band amplitude modulations in single trials reflected the behavioral choices made
206 by the animal, whether correct or wrong.
207
208 **Trial-by-trial correlations with task-related and spontaneous behavior differ for low and high**
209 **beta**
210 We adopted a Linear Model (LM) approach to further determine which of the task-related and
211 spontaneous behavioral factors (regressors) explained trial-by-trial amplitude variability in each beta
212 band, in a time-resolved manner across the different trial epochs. The task-related factors
213 encompassed the color condition, the RT and the direction of the upcoming reaching movement. The
214 spontaneous (uninstructed) variables included hand micro-movement velocity, eye velocity and gaze
215 position. We here only consider gaze In/Out of the work area, since preliminary analyses revealed no
216 systematic modulation of beta amplitude for gaze towards different items within the work area. We
217 also included the time-on-task as a regressor. The comparisons of 247 models (all combinations of
218 these 7 regressors and their 2-by-2 interactions) revealed that the winning model, with the lowest

219 Bayesian Information Criterion (BIC) in each 10ms bin along the trial, was mainly composed of a
220 single or a combination of several non-interacting regressors (Fig. 4B). Interaction terms were
221 present in the winning models in only 19/1360 bins (680 bins for each band). The direction of the
222 upcoming movement was almost always absent in the winning model except around and after the
223 GO signal for the low band. The eye velocity was also only sporadically part of the winning model.
224 Consequently, 5 LMs, each including one relevant regressor (color condition, RT, hand velocity, gaze
225 direction and time-on-task; excluding movement direction and eye velocity), were fitted separately
226 for the high and low beta bands. We chose to test each regressor separately, since in some sessions
227 one signal was not available or of poor-quality (mainly the eye signal). In a complementary analysis,
228 we fitted for each color condition separately a multi-regressor model including the 4 other variables
229 (RT, hand velocity, gaze position and time-on-task). In this complementary analysis, the importance
230 of each regressor in the full model was quantified by scrambling them across trials, one by one, and
231 determining the loss in total variance explained in the full model with the relevant variable
232 scrambled (Fig. S5). This complementary analysis largely confirmed the results described below.

233 The color condition explained trial-by-trial variability of both beta bands, also in this time-resolved
234 analysis (Fig. 4A). Importantly, the high band was modulated by the condition from SEL onset
235 (sample), and strongest around each SC (valid vs. distractor). The low band was modulated by the
236 condition only from the SC1 (blue) onset, due to the selective drop in amplitude after each valid SC.

237 The normalized RT did not affect the high beta band (Fig. 6A), but correlated positively with low
238 band amplitude, starting from each valid SC and up the GO signal (Fig. 6B). Thus, from the onset of
239 the cue that instructed the future movement, low beta amplitude reflected the level of preparation
240 of the upcoming reaching movement.

241 We next considered the spontaneous hand and eye movements. Hand velocity strongly explained
242 the trial-by-trial variability of beta amplitude, but almost exclusively for the low beta band (Fig 4C).
243 Low beta amplitude and hand micro-movement velocity correlated negatively during large portions
244 of the trial. The correlation was reduced around the presentation of each valid SC, and in the final

delay between SC3 (pink) and GO, in particular in the pink color condition. Despite the strong individual correlations of RT and hand velocity with low beta amplitude, the two behavioral factors were only sporadically correlated along the trial. Furthermore, a control analysis revealed that the variance in low beta amplitude explained by RT was not redundant with that of hand velocity (Fig. S6A).

To better understand the nature of this strong relationship between low beta amplitude and hand micro-movement velocity during the maintenance of central hold, we performed a cross correlation analysis (Fig. 6C). This analysis confirmed the strong negative correlation between hand velocity and low beta amplitude. It furthermore showed the temporal dynamics of these correlations. In the early trial epochs up to valid SC onset, beta was *lagging* the hand by 120-130ms. After valid SC onset, when low beta amplitude dropped (Fig. 4A), and subsequently hand velocity increased (Fig. 1C), cross correlations exhibited a wider pattern, with maximal negative correlation for 220-330ms in the direction of beta *leading* hand. This lag is comparable to the latency difference of 260-370ms between the moment of the steepest slope of the average beta amplitude decrease and the subsequent average hand velocity increase. The correlation with beta lagging the hand by 120-130ms remained, discernible as a 'shoulder' in the cross correlograms (Fig. 6F-H, top).

We next explored to which degree eye gaze direction (In/Out of the work area) affected beta amplitude. We quantified the correlation between gaze position (In/Out) and high and low beta amplitude at various temporal lags (Fig. S7A-B). A lag with gaze *leading* beta by 240 ms resulted in the largest number of correlated bins across both bands. At this 'optimal' lag, high beta amplitude was strongly affected by gaze position particularly in the trial epochs preceding the valid SC onset (i.e. different across the three conditions), and again just before the GO signal (Fig. 7A), with much stronger amplitude for gaze In. During valid SC, high beta amplitude was similar for gaze In/Out. Thus, the characteristic modulation in average high beta amplitude by the 'rhythmic' nature of the task was largely abolished when considering only gaze Out. Gaze position also influenced low beta band amplitude (Fig. 7B), however, the effect was less strong. The most consistent effect across the

three color conditions was a delay in the characteristic drop of low beta amplitude after the valid SC onset, for gaze Out. For both bands, the effect was much reduced or absent when considering other lags between gaze and beta amplitude (Fig. S7D-E). For the low band, we furthermore split trials according to gaze position taken at exactly 200ms after the valid SC onset. This confirmed that the drop in beta amplitude after the valid SC mainly occurred for trials with gaze In, compared to trials with the gaze still Out (Fig S7C).

Finally, for both beta bands the amplitude increased systematically with time-on-task (Fig. 8). A spectral parametrization analysis confirmed that amplitude increases were specific to the two beta bands and not caused by a change in the overall level or the slope of the aperiodic signal, which remained unchanged (Fig. S8). For the high band, the amplitude increase for late trials occured around SEL, and strongly and selectively in the delay immediately preceding each valid SC. For the low band, the amplitude increased within the session across most trial epochs, both before and after valid SC onset. We described above how RT was positively correlated with time-on-task, and furthermore that RT correlated positively with low beta amplitude between valid SC and GO. A control analysis revealed that the variance in low beta amplitude explained by RT described above was in part redundant with that of time-on-task (Fig. S6C).

DISCUSSION

We here describe a double-dissociation in sources and behavioral correlates of motor cortical low and high beta, with respect to both task-instructed and spontaneous behavior. In two macaques performing a delayed visuomotor reaching task, low beta dominated in M1, while high beta dominated in PMd. Low beta correlated positively with RT during preparation and negatively with uninstructed hand postural micro-movements throughout the trial. In contrast, high beta was unrelated to RT and hand postural dynamics, and instead modulated selectively in anticipation of and during visual cues, reflecting rhythmic temporal predictions. However, this rhythmic modulation was largely abolished when focal attention was oriented away from the work area. These clear-cut differences reconcile the many disparate roles proposed for the broader beta rhythm (~13-35Hz), designating specific roles in movement control for M1 low beta and spatio-temporal attention for PMd high beta.

Spontaneous hand and eye movements reflect movement preparation and focal attention

The monkeys performed a delayed match to sample task entailing strong working memory components, first for selecting the valid spatial cue (target) based on color matching, and second to memorize the target position while preparing the reach. Both monkeys performed spontaneous (uninstructed) hand and eye movements that were aligned to the task events. Such spontaneous movements were shown to persist even in highly constrained settings[33]. Our monkeys had to maintain their hand position within a very limited zone through most of the trial. Yet, they frequently made micro-movements with the hand, in particular during movement preparation. These spontaneous movements did not reflect the planned movement direction, but were possibly related to increased postural muscle tonus during movement preparation being imperfectly balanced across different muscles.

Furthermore, our monkeys were head-fixed, but free to move their eyes. They frequently shifted their gaze between items in the visual scene, or In and Out of the work area. We interpret these uninstructed shifts of gaze In/Out as reflections of spontaneous switches between covert attention

316 (gaze Out) vs. overt or focal attention (gaze In). In our task, trial start and GO were more than 6 s
317 apart, which is very long for maintaining focal overt attention. Having the gaze out of the work area,
318 which was more frequent before the valid cue presentation, probably reflected less focal attention
319 on the visual scene. The 'rhythmic' temporal predictability of the task events permitted shifting the
320 gaze to the work area in anticipation of or triggered by the salient visual events, in particular the
321 valid cue. This probably explains why the performance was correct even with periods of the trial
322 being monitored with peripheral vision and covert attention.

323 The neuronal activity was correlated with these spontaneous hand and eye movements to a
324 similar degree as with the task-instructed behavior.

325

326 **Low beta dominates in M1 and high beta dominates in PMd**

327 We found low beta to dominate in M1, while high beta dominated in PMd. Rather than a gradual
328 shift in peak frequency of a single beta band along the posterior-anterior axis, we observed two
329 distinct bands also at intermediate sites. Most studies of sensorimotor beta rhythms in monkeys
330 lumped frequencies from ~13-35Hz, such that any gradient across cortex might have been
331 overlooked. However, consistent with our result, Chandrasekaran et al.[30] found beta peak frequency
332 in PMd to be above 20Hz. Furthermore, near the central sulcus (including M1 and somatosensory
333 areas) beta was mainly observed to peak at or below 20Hz[47–52] (but see also[4,11]). Several studies of
334 beta rhythms in monkey prefrontal cortex reported peak frequencies above 20Hz[39,40,53–55]. Consistent
335 with this, Vezoli et al.[41] found high beta to be dominant anterior to low beta across the fronto-
336 parietal cortex in macaque ECoG. In humans, Rosanova et al.[56] showed that single-pulse transcranial
337 stimulation induced bursts of low beta in parietal cortex and high beta in premotor cortex, and
338 Mahjoory et al.[57] reported a gradual increase in beta peak frequency along the posterior-anterior axis
339 in resting state magnetoencephalography. It is therefore probable that the low and high beta bands
340 that we here characterize across motor cortex extend well beyond, and at the cortical level reflect a
341 low beta network including M1, somatosensory and parietal regions and a high beta network

including PMd and prefrontal regions, not excluding further involvement of also subcortical structures such as the basal ganglia[46,48,58].

The distinctly different temporal profiles of M1 low and PMd high beta amplitudes were mirrored in the very different temporal profiles of average MUA amplitude when split according to beta band dominance. This suggests a functional split across the motor cortex, with band-specific roles in movement control and spatio-temporal attention, respectively. Note however that individual neurons have very diverse activity profiles in such visuomotor tasks[27], and some rather inverse to the average MUA amplitude profile. Furthermore, there is no trial-by-trial correlation between the firing rate of individual neurons and beta amplitude[28].

Low beta reflects movement preparation and continuous postural dynamics

Many studies described a decrease in sensorimotor beta amplitude during movement preparation[23], but here we show this to be restricted to the low band, following the valid spatial cue. Lack of focal attention at the time of the valid cue onset (gaze Out) delayed this amplitude drop, and possibly also the onset of movement preparation. Along with the negative correlation with spontaneous hand micro-movements and the positive correlation with RT, these are strong evidences for M1 low beta reflecting movement preparation and postural control processes. In contrast, the amplitude of the high beta band in PMd was largely independent of hand micro-movements and behavioral RT, and remained high during movement preparation. The drop in average low beta amplitude after valid cue onset was accompanied by an inverse modulation in the average amplitude of local MUA, which increased after valid cue onset. This underscores the importance of low-beta dominant cortical sites in movement preparation processes.

Time-on-task effects were attributed to increased cognitive effort or decreased vigilance in attentionally demanding tasks[29,42]. Consistent with this, we found that behavioral RT increased with time-on-task. The RT was furthermore positively correlated with low beta amplitude, but only during movement preparation, not prior to the valid spatial cue presentation. Low beta amplitude was also positively correlated with time-on-task, across all trial epochs. A control analysis revealed that RT was

369 partly redundant with time-on-task in explaining low beta amplitude. As RT only affected low beta
370 amplitude during movement preparation, taken together these results suggest the time-on-task
371 effects reflected increased cognitive effort related to postural control and movement preparation,
372 rather than a non-specific decrease in vigilance.

373 A recent study reported transient beta bursts even during sustained isometric gripping in humans
374 [59], suggesting no direct link between cortical beta amplitude and motor output. The spontaneous
375 hand postural micro-movements we observed were 100-fold smaller in velocity than the center-out
376 reaching responses (Fig S1A), yet strongly correlated with low beta amplitude across all trial
377 epochs. The discrepancy between their and our findings might be due to the large number of trials
378 available for our analysis, or less sensitivity in their setup for detecting minute changes in grip force
379 during the sustained isometric contraction.

380 The negative correlation between low beta and hand velocity was maximal for beta lagging hand
381 by about 120-130 ms prior to the valid cue (Fig. 6C). In comparison, directed descending and
382 ascending coherence in the beta frequency range between cortex and muscle [60,61] were reported to
383 have much shorter phase delays than this, on the order of 25 ms. Instead, Jasper and Penfield[1]
384 already speculated whether the emergence of sensorimotor beta bursts reflects a "state of
385 equilibrium of activity permitting again a synchronization of unit discharge". This could be an
386 equilibrium between excitation and inhibition[62], with beta reflecting the network resonance
387 frequency[56,57,63–65]. In this view, a decrease in M1 low beta amplitude *lagging* an increase in hand
388 micro-movement velocity might reflect a shift away from neuronal population activity equilibrium,
389 with the explicit aim to prevent the hand cursor from sliding outside the central fixation spot, since
390 this would abort the trial.

391 During movement preparation the correlation with beta lagging hand persisted, but low beta
392 amplitude and hand velocity here correlated negatively across a broad range of lags, with maximal
393 correlation strength for beta *leading* the hand of 220-330ms. This lag is close to, and presumably

394 dominated by, the average temporal difference of 260-370ms between the drop of low beta and the
395 subsequent increase in hand velocity.
396
397 **High beta reflects temporal task prediction and focal attention**

398 Beta amplitude modulations scale to predictable delay durations in visuomotor tasks[20,22]. We
399 found that whereas the condition selectivity in the low band only emerged during movement
400 preparation, the high band was already selective before the first spatial cue, in a predictive manner.
401 Beta amplitude in frontal cortex was found to modulate with 'rhythmic' visuomotor or working
402 memory tasks[18,39] and passive auditory tasks[19] permitting rhythmic temporal predictions. We here
403 demonstrate that rhythmic beta amplitude modulations related to temporal prediction and attention
404 were restricted to the high band and were much enhanced during focal attention towards the work
405 area (gaze In), in particular in the delays leading up to the presentation of the valid cue.

406 The rhythmic amplitude modulations we here describe for PMd high beta strongly resemble those
407 reported by Lundqvist et al.[39] for macaque prefrontal cortex high beta during a working memory task
408 requiring central eye fixation (i.e. comparable to *gaze In* for our study) and saccade responses. A
409 phase locking analysis confirmed that the high beta band we observed in the PMd sites was locally
410 generated. Furthermore, the average amplitude of local MUA in high beta dominant sites modulated
411 inversely to the high beta amplitude (as were also gamma bursts and neuronal firing rates in[39]), and
412 peaked during the processing of valid visual spatial cues. The similarity of high beta amplitude
413 modulations for these two experimental settings suggests a general role in effector-independent
414 spatio-temporal prediction and attention in frontal cortex. High beta amplitude increased with time-
415 on-task, but mainly during SEL cue presentation and in a condition-dependent manner in the delay
416 immediately preceding and during the valid cue. This might reflect increased allocation of spatio-
417 temporal attention towards the most relevant visual cues (SEL and valid SC), as the animal
418 fatigued[29,42].
419

Conclusion

Sensorimotor beta rhythms remain enigmatic, despite 75 years of scientific efforts since Jasper and Penfield[1] first speculated whether beta bursts might reflect states of neuronal activity equilibrium. Here, by designing a demanding visuomotor task and by considering task-related, but also spontaneous behavior, we describe a double-dissociation in sources and behavioral correlates of low and high beta rhythms within the motor cortex. Our clear-cut findings reconcile the largely disparate roles proposed for sensorimotor beta, ranging from movement inhibition to temporal expectation[23]. By acknowledging that the motor cortex contains multiple beta rhythms with band-specific behavioral and cognitive correlates, we can advance towards their complete understanding.

MATERIALS AND METHODS

Animal preparation

Two adult male Rhesus monkeys (T and M, 10 and 14 kg, respectively) participated in this study. Care and treatment of the animals during all stages of the experiments conformed to the European and French Government Regulations (2010/63/EU; authorization identifier 03383.02). Previously published studies using data from these two monkeys[20,27,28,66–68] were based on recordings from the opposite hemisphere during performance of another visuomotor task.

Subsequent to learning the visuomotor task (see below) the monkeys were prepared for multi-electrode recordings in the left hemisphere of the motor cortex (M1 and PMd), contra-lateral to the trained arm. In a first surgery, prior to completed task learning, a titanium head-post was implanted posteriorly on the skull, fixated with titanium bone screws and bone cement. In a second surgery, several months later, a cylindrical titanium recording chamber (19mm inner diameter) was implanted. The positioning of the chamber above upper-limb regions of M1 and PMd was confirmed with T1-weighted MRI scans (prior to surgery in both animals, and also post-mortem in monkey M), and with intra-cortical electrical microstimulation (ICMS; as described in [69]) performed at the end of single-tip electrode recording days in the first recording weeks, in both monkeys. The recording sites included in this study spanned about 15mm across the cortical surface in the anterior-posterior axis, and only include sites determined with ICMS to be related to upper limb movements (Fig. 3C). The exact border between PMd or M1 areas was not estimated.

Behavioral setup and task

Two monkeys were trained to perform a visuomotor delayed match to sample task with fixed cue order and a GO signal (Fig. 1B). The task required arm-reaching responses in one of 4 (diagonal) directions from a common center position, performed by holding a handle that was freely movable in the two-dimensional horizontal plane. The visual scene was displayed on a vertical computer monitor (LCD; 75 Hz) in front of the monkey (Fig. 1A). We here describe the monitor stimuli in cm units, but

since the viewing distance was about 57 cm, this approximates to the same degrees of visual angle. Before the start of each trial, the monitor displayed the handle (hand cursor) position (small white square; 0.4cm edges), a central fixation spot (yellow flashing disc; 0.45cm radius), and the 4 possible peripheral target positions (red circular outlines; 1.5cm radius at 9 cm diagonal distances from the center). The position of the cursor was updated on the monitor every 40ms (~every 3rd frame), but only if the accumulated displacement from the previous update exceeded 0.1cm (to avoid flicker due to electronic noise).

The monkey initiated the trial by positioning the cursor inside the central hand fixation spot. This central touch ended the flashing of the fixation spot (which remained on), and was accompanied by an auditory tone, presented for 50ms. After holding this central position for 1000ms, a selection cue (SEL) indicating the color to attend for that trial appeared on the screen for 300ms, displayed behind but extending well beyond the central yellow disc and the overlying hand cursor. SEL consisted of one out of three differently colored polygons (blue, green or pink; ~3cm radius) defining the color condition. A 1000ms delay followed SEL offset. Thereafter, three peripheral spatial cues (SC1-3) were presented in sequence, each displayed for 300ms, with 1000ms delay after each of them. The SCs were colored discs (0.9cm radius), always presented in the temporal order blue-green-pink, each within one of the 4 peripheral red outlines.

All 4 diagonal target positions were equally likely for each SC. Thus, successive SC in the same trial could be presented in the same position. This resulted in 192 unique trials, combining the 3 color conditions with the 4 independent positions for SC1, SC2 and SC3. In monkey T, who was not willing to work for as many trials as monkey M, only 3 of the 4 target positions were used in each session (randomly selected for each session), to reduce the number of unique trials. For both animals, to ease the task, the three color conditions were presented separately in small blocks of approximately 15 unique trials per block, cycling across multiple blocks of the three color conditions to complete all the unique trials. The unique trials within each block were presented in pseudo-random order.

482 Incorrect trials within a block were re-presented later in the same block, and each block was
483 completed only when all unique trials in the block were correctly executed.

484 The animal had to select the (valid) SC according to the color indicated by SEL (i.e. delayed color
485 match to sample), and ignore the two (distractor) SCs of different colors. The GO signal was
486 presented after the final 1000ms delay following SC3, prompting the animal to execute the center-
487 out arm reaching movement to the memorized valid SC position. The GO signal was directionally
488 non-informative, consisting in the simultaneous onset of 4 red light-emitting diodes (LEDs;
489 embedded in a thin Plexiglas plate in front of the monitor) at the centers of the 4 circular target
490 outlines. The reaction time (RT) and movement time each had a maximum allowance of 500ms. The
491 animal was trained to stop and 'hold' within the correct peripheral target outline for 300ms to obtain
492 a reward. The touch of the valid target was signaled by an auditory tone (50ms) and a completed
493 hold with another tone (50ms). Reward was delivered 500ms after completed hold, and consisted in
494 a small drop of liquid (water or diluted fruit juice). Monkey T was not rewarded for non-hold trials,
495 while monkey M was given a smaller reward on non-hold trials (on the valid target; 500ms after
496 breaking hold). For both animals, these non-hold trials were included in the analysis (about 10% of all
497 included trials).

498 The manual (horizontal) work area of the monkey was scaled down with respect to the display on
499 the monitor (by a factor of about 0.7). In manual (horizontal) space, the diagonal distance (center to
500 center) between the fixation spot and peripheral targets was 6.5cm. The required central fixation
501 zone was defined to be within a radius of 0.3cm, and the accepted touch zone of the peripheral
502 targets had a radius of 1cm. These touch zones corresponded to the hand cursor overlapping more
503 than halfway with the fixation spot or the peripheral outlines. In the offline analysis of the hand
504 signal, we used the spatial scaling of the visual scene on the computer monitor.

505 In short, in this delayed match to sample task, the timing and sequential order of the three SCs
506 were fully predictable, and SC validity was cued at the start of each trial by SEL. Only the spatial
507 positions of the three SCs were unpredictable.

508

509 **Data acquisition**

510 During recording days (maximally 5 days a week), a multi-electrode, computer-controlled
511 microdrive (MT-EPS, Alpha Omega, Nazareth Illith, Israel) was attached to the recording chamber and
512 used to transdurally insert up to five single-tip microelectrodes (typical impedance 0.3-1.2MΩ at
513 1,000Hz; FHC) or up to two linear microelectrode arrays (either V- or S-probes, Plexon, Dallas, TX,
514 USA or LMA, Alpha Omega; each with 24 or 32 contacts, inter-contact spacing either 100, 150 or
515 200µm; 12.5 or 15µm micrometer contact diameters) into motor cortex. In this study we employ the
516 term 'site' for the recording obtained from each individual single-tip electrode (or from each linear
517 array) recorded in individual behavioral sessions. The electrodes (or arrays) were positioned and
518 lowered independently within the chamber (Flex-MT drive; Alpha Omega) in each session. Individual
519 guide-tubes for each electrode/array were used that did not penetrate the dura (no guide was used
520 for the more rigid LMA array). For single-tip electrodes, the reference was common to all electrodes
521 and connected, together with the ground, on a metal screw on the saline-filled titanium recording
522 chamber. For the linear array recordings, the reference was specific to each array type. For the LMA
523 (Alpha Omega) it was an insulated wire exposed at the tip, either emerged in the chamber saline, or
524 attached with a crocodile clip to the probe stainless steel tube (which in turn was lowered into the
525 chamber liquid, but not extending into brain tissue). For the V- and S-probes (Plexon) in most cases
526 the reference was the stainless steel shaft of the array (extending into brain tissue, in near proximity
527 to the probe's recording contacts). In a few sessions, the reference was instead placed on a skull-
528 screw on the more posterior headpost (7/41 sites using v-probes in monkey T) or on a screw on the
529 saline-filled recording chamber (1/51 sites using s-probes in monkey M). For both array types, the
530 ground was either connected to a skull-screw of the remote titanium head-fixation post, or to a
531 screw of the titanium recording chamber.

532 We used two different data acquisition (DAQ) systems to record neuronal and behavioral data. All
533 single-tip electrode recordings in monkey T were obtained on a recording platform with components

534 commercialized by Alpha Omega. This system included the Alpha-Map system for online monitoring
535 of signals (running on Windows XP), and the MCP-Plus multi-channel signal processor including
536 analog head-stages. Neuronal signals from each electrode were amplified with a gain of 5,000 to
537 10,000 (with unit-gain head-stage), hardware filtered (1Hz – 10kHz) and digitized and saved for
538 offline analysis at a sampling rate of 32 kHz.

539 All linear array recordings in monkey T, and all recordings (single electrodes and linear arrays) in
540 monkey M, were obtained on a recording platform with components commercialized by Blackrock
541 Neurotech (Salt Lake City, UT, USA). This system included Cereplex M digital head-stages (versions PN
542 6956, PN 9360 and PN 10129) connected to a Digital Hub (versions PN 6973, PN 6973 DEV 16-021, PN
543 10480) via custom HDMI cables (versions PN 8083, PN 8068), which transmitted signals via fiber
544 optics to a 128 channel Neural Signal Processor (NSP hardware version 1.0), and control software
545 Cerebus Central Suite (v6.03 and v6.05 for monkeys T and M, respectively; running on Windows 7).
546 An adapter (PN 9038) permitted connecting multiple single-tip electrodes to the Cereplex M
547 Omnetics connector (Monkey M). Neuronal signals were hardware filtered (0.3Hz – 7.5 kHz) and
548 digitized and saved for offline analysis at a sampling rate of 30 kHz.

549 Behavioral event codes (TTL, 8 bits) were transmitted online to the DAQ system from the VCortex
550 software (version 2.2 running on Win XP; NIMH, http://dally.nimh.nih.gov), which was used to
551 control the behavioral task. A custom rebuild of the VCortex software allowed simultaneous online
552 monitoring of hand and eye gaze positions in the common reference frame of the animal's visual
553 monitor display. Continuous hand position (X and Y) was obtained from two perpendicularly
554 superimposed contactless linear position magnetorestrictive transducers, model MK4 A; GEFRAN,
555 Provaglio d'Iseo, Italy). The 'floating' magnetic cursor was attached to a manipulandum that could be
556 moved along two pairs of rails with ball bearings, each pair aligned with one of the two transducers.
557 The Y-oriented rails were fixed on top of the X-oriented rails. As such, this system provided
558 somewhat less frictional resistance in the Y direction than in the X direction. Furthermore, either of
559 the uni-directional X or Y displacements provided somewhat less frictional resistance than their

560 combination needed to move to the diagonally placed targets. Hand position was used online to
561 control the behavioral task. The hand position was also saved by VCortex for offline analysis (at
562 250Hz sampling rate). In a majority of sessions, eye gaze position (X and Y) was recorded by the DAQ
563 system (video based infrared eye-tracking; RK-716PCI (PAL version) at 50Hz for the first single-tip
564 electrode recordings in monkey T, or ETL-200 at 240Hz sampling rate for the array recordings in
565 monkey T and all recordings in monkey M; ISCAN Inc., Woburn, MA, USA). The eye-tracking camera
566 was positioned next to the lower right corner of the monkey's computer monitor.

567 In many sessions we also recorded heart rate (plethysmographic pulse waveform from ear-clip
568 pulse oximeter, model 8600V; Nonin Medical Inc, Plymouth, MN, USA), and in some sessions surface
569 electromyogram (EMG) from one or two proximal upper limb muscles (deltoid/biceps).

570

571 **Statistical analysis of behavioral performance**

572 All analyses of behavioral and neuronal data were conducted offline by using Matlab (The
573 MathWorks, Inc.) and Python. Multiple comparison chi-squared tests using the Matlab function
574 crosstab were used to compare percentages of distractor errors for the three color conditions and
575 the four movement directions. 3-way ANOVAs were used to quantify the variability in RT across
576 sessions, color conditions and movement directions for each monkey. Finally, to determine whether
577 there was any systematic within-session modulation of RT, we normalized (z-scored) the RT within
578 each session (to compensate for any differences in average RT across sessions), before collapsing
579 trials across all sessions for each monkey. We then calculated the Pearson correlation coefficient
580 between RT and trial number inside each session.

581

582 **Hand position analysis**

583 The hand position signals that were recorded with VCortex were realigned in time with the other
584 data recorded by the DAQ system offline, by realigning the behavioral event codes and up-sampled
585 (linear interpolation) from 250Hz to 1kHz. The hand position signals were calibrated (scaled) online in

586 the VCortex configuration to match the visual display before storing on file, and in analysis we used
587 the spatial scaling of the visual scene in cm.
588 The RTs for the center-out reaching movements were redefined offline using the hand
589 trajectories. First, hand velocity and acceleration were computed in each trial, using a Savitsky-Golay
590 algorithm. To determine reach movement onset, in a 2000ms duration epoch centered on GO,
591 periods with prolonged increased velocity (>50ms) above an empirically determined velocity-
592 threshold (6 cm/s) were then detected, and the final, preceding increase in acceleration above an
593 empirically determined acceleration-threshold (6 cm/s/s) was then taken as the time of movement
594 onset. These RTs were confirmed in both animals by visual inspection of single trial trajectories in
595 several sessions.
596 We also quantified hand micro-movements during the maintenance of stable central hand
597 position using hand velocity and position.
598
599 **Eye position offline calibration and analysis**
600 In a majority of sessions we recorded eye position with an infrared camera. A rough online
601 calibration of the gain and offset of the eye X and Y signals were done during the first behavioral
602 trials in each recording session, to compensate for small changes in head fixation or camera position
603 compared to the previous day/session. This simplified online calibration was adopted to avoid
604 training the monkey in a fixation task. The center of gaze was set to zero (center) while the monkey
605 looked at the small yellow central target in order to place the hand cursor therein to initiate a new
606 trial. Then, on some days the X or Y gain was updated slightly so that the spontaneous eye fixations
607 on the peripheral target outlines matched their position in the Cortex software interface. The trials
608 before calibration (typically 0-3 correct trials) were excluded in offline analysis involving eye
609 movements.
610 For data analysis, the eye signals recorded with the DAQ system were re-calibrated offline, to
611 correct for the distortion induced by having the camera off the horizontal and vertical central axes of
612 gaze. First, the raw eye signals were inspected visually to exclude from offline calibration and analysis

613 the trials that were recorded before the completion of the rough online calibration, typically
614 consisting in suppressing the 0-3 first correct trials in each session. Raw data were downsampled
615 from the acquisition sampling frequency (1 or 30 kHz) to the camera sampling frequency (50 or
616 240Hz) and linearly rescaled from bits to volts. We computed the eye velocity in volts/s using the
617 Savitzky-Golay algorithm. For the offline calibration algorithm, we only considered data points that
618 likely belong to fixation periods (i.e. whose velocity was lower than the lower 10th percentile of the
619 total velocity distribution). At this stage, the superimposition of eye positions during these low
620 velocity epochs across all trials in a session already showed an expected clustering of the data around
621 5 positions on the screen whose geometry resembled the center and 4 peripheral target positions
622 used in the task. Thus, we were able to define boundaries in the voltage space to separate data
623 points according to whether they were recorded when the monkey was looking within the work area
624 (approximate boundaries of computer monitor) or when he was looking away from the work area
625 (e.g looking in the ceiling, or signal saturation due to eye blinks). The low velocity (fixation) data
626 occurring within the work area was then sorted into 5 clusters using a k-means algorithm (kmeans
627 function in MatLab, using squared Euclidean distance). Cluster centers were assumed to represent
628 the target positions in the voltage space. We next generated a 2D non-linear model to compensate
629 for the distortion due to camera position, between target coordinates on the screen (in cm) and
630 voltage amplitudes of the corresponding centroids. This was achieved by adjusting a polynomial
631 function to fit the relationship between each coordinate in the screen space to the XY coordinates in
632 the voltage space. The correction was then applied to the complete eye traces. A detailed version of
633 this correction can be found in[70]. Each data point was re-assigned to a cluster if it was located at a
634 distance <2cm from the target's center coordinates, or assigned as being between clusters (but
635 within the work area), or outside of the work area (incl. saturated). Eye position, velocity and
636 acceleration were then saved for further analysis, scaled in cm of the visual display, alongside cluster
637 membership of each data point. Furthermore, the data points outside the work area that were

638 beyond the lower or upper 0.99 percentiles of the boundaries of the raw X and Y voltage signals were
639 marked as 'saturated'.

640 To detect the saccadic eye movements, we applied a recursive algorithm that seeks for the largest
641 breakpoint in a piecewise stationary process, in a trial-by-trial fashion. First we computed the
642 cumulative 2D velocity of the eye signal in cm/s. This representation yields a pseudo staircase profile
643 alternating between steep and slowly increasing periods over time. We extracted the highest decile
644 of the velocity distribution and marked the corresponding steps in the staircase as boundaries to
645 define periods when the subject was looking coarsely in the same area. These steps corresponded to
646 blinks or to obvious large saccades and the steady periods were either fixation periods or multiple
647 fixation periods with intermittent smaller saccades. During the steady periods, the cumulative
648 distribution showed a slow increase due to noise originating from micro-movements and the
649 recording device. The contribution of this noise being dependent on the location of the fixation on
650 the screen, we compensated for it by subtracting the average slope for each period separately. This
651 gave a piecewise stationary process that showed pseudo-horizontal steady epochs with better signal
652 to noise ratio for the intermittent smaller saccades. Secondly, we applied a recursive algorithm to
653 this process consisting, within a given time window, to compute at each data point the difference
654 between the prior and the posterior average values. The maximum difference was extracted and
655 compared to a threshold value computed after the velocity profile of a reference saccade (10ms
656 duration, 60cm/s velocity peak). If the maximum difference was larger than the threshold, it was
657 considered an actual transition and the time window was split in two at this time point. Starting with
658 a time window covering the whole trial, the algorithm defined new (smaller and smaller) time
659 windows at each iteration and the new window boundaries were considered as transitions. To avoid
660 transitions to be detected multiple times, we introduced a 'refractory period' of +/-15ms around
661 accepted transitions. Fixation periods were finally defined by sorting the transitions between
662 fixations into detected saccades or detected micro-saccades depending whether or not the euclidian
663 distance between the isobarycenter of two successive fixations was larger than a threshold (the

change in eye position on the screen for an eye movement of 0.5cm). Saccade onset/offset times were saved for further offline analyses alongside the other calibrated eye signals detailed above.

Finally, eyeblinks were detected as two subsequent (<150ms apart) eye signal velocity passings beyond a velocity threshold (500cm/s for the 50Hz sessions and 800cm/s for the 240Hz sessions). The data points in a window including the gap between these subsequent threshold passings, as well as a couple of preceding and subsequent flanker data points were marked as eyeblinks. Visual inspection confirmed that this method was able to distinguish between saccades and abrupt velocity increases due to eyeblinks, even if large standalone saccades sometimes had velocities beyond the thresholds used for eyeblink detection.

LFP spectral analysis and beta amplitude extraction

All sessions with sufficient quality of data were included in analysis. The raw signals were low-pass filtered offline at 250Hz cut-off frequency (zero-phase 4th order Butterworth filter, using the butter and filtfilt functions in Matlab) to obtain the LFP signal, which was then downsampled to 1KHz and saved for further analysis. For this study, we included only one contact for each of the linear array penetrations, selected to be well within cortex and with low noise (e.g. no heartbeat artifacts). LFP activity from 110 individual sites (63 with single-tip electrodes and 47 with linear arrays) in 59 sessions monkey T and 60 sites in 39 sessions (10 with single-tip electrodes and 50 with linear arrays) in monkey M were included in the analysis. A site is here defined as the conjunction of a specific chamber coordinate of the electrode entry and cortical depth, in one recording session. In the included LFP sites, trials with obvious artifacts (mainly due to teeth grinding, static electricity or heart-beat signal) detected by visual inspection, were excluded from further analysis (12.3% of all trials in monkey T and 5.1% in monkey M). As the duration for which the monkeys were willing to work varied across sessions, after trial exclusion, the analyzed sites included on average 96.4 +/- 48.8 (STD) trials (range 19-184) in monkey T, and 147.3 +/- 80.3 trials (range 18-281) in monkey M. We

689 also included the sites with few trials, since a majority of the neuronal data analyses were done on
690 trials collapsed across many sites.

691 Power spectral density (power for short) estimates of the LFP were obtained using the Pwelch
692 function of Matlab. For LFP spectrogram examples (Fig. 2A-C), we highpass filtered the LFP with 3Hz
693 cutoff, using a 4th order Butterworth filter. Power was estimated for single-trial sliding windows of
694 300ms duration, with 50ms shifts, at 1Hz resolution, before averaging across trials.

695 For average spectrograms for each monkey (Fig. 2E), we also used 300ms sliding windows, 50ms
696 shifts, at 1Hz resolution. For each individual LFP site, we first highpass filtered the signal (3Hz cutoff,
697 4th order Butterworth filter), before calculating the power for each window in single trials. Next, the
698 power matrix (trial x window x frequency) for each LFP was normalized by dividing by the mean
699 power between 10-40Hz across trials and windows for that LFP. We then computed for each window
700 the grand average power across all individual trials for all normalized LFPs (i.e. each trial contributed
701 equally to the grand mean, independent of the total number of trials for the specific LFP site). For
702 single site and average spectrograms we used a perceptually flat color-map[71], with color limits set to
703 the minimum and maximum power values between 12-40Hz between onset of SEL and GO,
704 separately for each site or each monkey.

705 To determine the peak frequencies of the two observed beta bands, we estimated power in a
706 900ms epoch preceding SC1 (blue) onset, across all trials for each LFP site (after highpass filtering at
707 3Hz ; 4th order Butterworth filter). Within this epoch, we used five 500ms windows, with overlap of
708 400ms, to get one average power estimate per trial. We then normalized the power matrix (trial x
709 frequency) for each LFP by dividing by its mean power across trials between 10-40Hz. To have a 'fair'
710 comparison of power across the two beta bands, despite the 1/f nature of the aperiodic signal
711 component, the aperiodic signal component was removed in each site independently, before
712 averaging across all trials of all sites and plotting the grand average spectral power (Fig. 3A). In order
713 to estimate (and remove) the aperiodic component of the signal, we used an approach similar to
714 FOOOF[72]. Preliminary analysis using the standard FOOOF method showed that it was not estimating

715 adequately the aperiodic component of the spectrum, presumably due to high power in the lower
716 frequencies. Following their assumption that in a restricted frequency range the aperiodic
717 component is a straight line in the log-log space, and since we were interested in parametrizing the
718 power only for the beta range, we decided to adapt their method to our specific need. We first
719 computed the logarithm of the power of all single trials in each site. Once in the log-log-space, we
720 calculated the average power per site and looked for two local minima; the last minimum before 10
721 and the last minimum before 50Hz. The aperiodic component was estimated by a straight line
722 connecting the two minima, and then removed from each single trial in that session. In the case one
723 of the two local minima were not present in a session, the first line point was set at 10Hz, and the
724 second in the minimum value between 35-50Hz.

725 We also determined, for each individual trial, the frequency between 10 and 40Hz with maximal
726 power (beta peak frequency) in the periodic-only component of the signal (Fig. 3A). Based on these
727 distributions of power and peak frequencies, for both monkeys a range for the low band of 13-19Hz
728 and for the high band of 23-29Hz were used to determine the dominant beta band for each LFP site.
729 We computed a beta band dominance index using mean power in the periodic-only signal
730 component across all trials and frequencies in the low band minus mean power across all trials and
731 frequencies in the high band, divided by the sum of the two. Significance in band dominance was
732 determined with a paired t-test across trials, taking the mean power across all frequencies in each
733 band for each trial (Fig 3C).

734

735 **Phase-locking of neuronal spiking to LFP beta phase**

736 To verify that the LFP beta bursts were at least partially of local origin, we analyzed phase-locking
737 of the simultaneously recorded neurons to the LFP beta phase of the site-dominant band. We
738 included only the laminar recording sites, and tested phase locking for neurons across all laminar
739 contacts to the LFP on the selected LFP contact on the same laminar probe, to ensure proximity of
740 the two signals. We analyzed the delay before SC1 (blue), since the beta amplitude was generally

741 strong in both animals and in both bands in this delay. Only neurons with more than 100 spikes in
742 this delay, accumulated across all trials, were included. Beta phase was extracted from the Hilbert
743 transformation of the beta-filtered LFP, only for the dominant beta band at each LFP site, and the
744 phase at each spike time was determined.

745 To quantify the phase locking, we first used Rayleigh's test of non-uniformity of circular data[73]. To
746 determine whether the locking was significant for individual neurons, a trial-shuffling method was
747 used. Trial-shuffling is an efficient method for obtaining a 'baseline' measure of phase locking,
748 destroying the direct temporal relationship between the two signals, while preserving their individual
749 properties such as rhythmicity and dependencies on external (task) events. 1000 repetitions of the
750 phase-locking analysis (Rayleigh's test) was done while randomly combining beta phases and spike
751 times from different trials. If the original data yielded a larger z-statistic value from the Rayleigh's
752 test than 950/1000 (equivalent to $p<0.05$) of the trial-shuffled controls, the phase-locking of the
753 neuron was considered significant.

754

755 **Decoding task condition with beta amplitude**

756 First, a two-dimensional reduction visualization (t-distributed Stochastic Neighbor Embedding; t-
757 SNE) was used to explore whether the different color conditions were separable in each of the two
758 beta bands (see insets in Fig. 5A). Second, we built two classifiers using high and low beta bands
759 separately, to decode color conditions. For each, the features were extracted from the temporal
760 evolution of beta amplitude in single trials. We calculated the average beta amplitude in 50ms non-
761 overlapping time bins from touch to GO in each trial. A random forest estimator from scikit-learn
762 library[74] was trained in the data. Using gridsearch, we found the parameters which maximized
763 classifier performance for both frequency bands (max_depth=80, max_features=3,
764 min_samples_leaf=3, min_samples_split=8, n_estimators=200). Unambiguous correct trials (trials in
765 which none of the distractors were presented in the same quadrant) were split in a 60-40% ratio
766 between train and test set, respectively. To ensure stability of the method, we repeated the

procedure using 20 different data splits, always with class balance in the train set. The average performance for each of the classes was computed by averaging across repetitions. After training the classifier on the unambiguous correct trials, the same model was used to predict distractor error trials (only including the trial in which the two distractors were not presented in the same quadrant). In this case, we predicted either the color of the attended (distractor) SC, or the color of SEL; i.e., either the SC the monkey actually used, or the SC the monkey should have used. The chance level was calculated by shuffling the labels in 100 train-test splits of the data for both high and low beta classifiers. All the accuracy values estimated in the different shuffle test-sets were below 0.37, which we set as the overall chance level for the results.

LM and cross-correlation analysis to quantify the relationship between beta amplitude and behavioral regressors

Dataset preprocessing

Given the similarity in the behavioral and neuronal data from the two animals up to this point, for all subsequent analyses we combined LFPs for both monkeys, while splitting low and high band dominant sites. We furthermore continued the analyses using the single-trial instantaneous beta amplitude. For each LFP site, we first bandpass filtered the signal to extract the dominant beta band, either 16+/-4Hz for low dominant sites or 26+/-5Hz for high dominant sites, using 8th order Butterworth filters. We next calculated the instantaneous amplitude (envelope) of the beta filtered LFP time series by constructing the analytic signal using the Hilbert transform. The LFP was then cut in trials, before normalizing the beta amplitude by subtracting the grand mean amplitude and dividing by the grand amplitude standard deviation. After normalization, individual trials for all LFP sites with the same beta band dominance were lumped to construct large matrices (trials x time) for each of the two beta bands, combining data from the two monkeys (Fig. 4A).

The eye signals (position and velocity) were upsampled to 1KHz, to have the same temporal resolution as the LFP and hand signals. The eye velocity was upsampled using a linear interpolation

793 whereas the position of the gaze in the different clusters of the work area was upsampled using the
794 nearest neighbor interpolation.

795 *Bayesian Index Criterion*

796 To evaluate the relation between complementary continuous and categorical variables with the
797 LFP signal, we performed a Linear Model (LM) analysis. The LFP from both low and high beta bands
798 were the variables to explain. The regressors considered to explain the data were 7 : color conditions
799 (3 levels), movement direction (correct target location, 4 levels), reaction time (normalized with a z-
800 score inside each recording session), time-on-task (computed with the relative position of the trial
801 within the recording session), hand velocity (cm/s), eye velocity (cm/s) and the gaze position of the
802 animal (inside vs outside the work area, 2 levels) and all 2-by-2 interactions. More complex
803 interactions were excluded from the model to simplify the interpretation of the results and reduce
804 the number of potential regressors. We considered a total of 6800 ms, from -1200ms to 5600ms
805 from the SEL for the analysis. All the neuronal and behavioral data were then binned in 10ms non-
806 overlapping windows. In each bin we applied a total of 247 models (all combinations of 1 to 7
807 regressors including or not their 2-by-2 interactions) and compared them using a Bayesian Index
808 Criterion (BIC). The BIC is sensitive to the number of trials considered in each model fitting.
809 Consequently, we applied the same selection for each model, removing from all bins the trials in
810 which the eye or the hand signals were missing, and furthermore removing trials in individual bins if
811 the eye signal was saturated because of an eyeblink or an extreme eye position outside the dynamic
812 range of the eye camera. We then examined the presence or not of a regressor and or interactions in
813 the winning model in each of the 680 bins. This first analysis allowed us to target the regressors
814 explaining the most trial-by-trial variability of high and low beta amplitude (Fig. 4B).

815 *Linear Model Analysis*

816 Based on the BIC analysis, 5 regressors, without interactions, were selected. Movement direction,
817 eye velocity and all the possible pairwise interactions were discarded because they were rarely
818 represented in the regressors best explaining the beta. The trial selection was different for each

819 selected regressor, based on available trials for each regressor. All trials could be used for color
820 condition, RT and time-on-task (trial number within each session) regressors. Good quality of the
821 hand signal was necessary for the hand velocity regressor. Good quality of the eye signal was
822 necessary for the gaze position. For gaze position, the eyeblinks were considered as outliers and the
823 corresponding single-trial bins with an eyeblink were removed for the model fitting. The different
824 number of trials available considered for each bin and each regressor prompted us to consider each
825 regressor separately. For each bin, each regressor and each beta band, we applied a regression
826 model (*fitlm*) to describe the relationship between beta amplitude and the 5 different predictors. The
827 color condition was applied considering all conditions together. The other models were applied
828 considering each color condition separately. Considering that some variables were categorical, we
829 applied an ANOVA to the model objects to test the significance of the categorical variables. P-values
830 <0.01 were considered significant.

831 *Two-dimensional cross correlograms between hand velocity and low beta amplitude*

832 An analysis equivalent to the joint peristimulus time histogram (eq-jpsth) representation of the
833 cross-correlation between two neurons[75,76] was performed using the Fieldtrip toolbox[77]. Instead of
834 the activity of 2 simultaneously recorded neurons, we used hand velocity and low beta amplitude as
835 input signals. The eq-jpsth corresponds to the 2-dimensional cross-correlograms. Time versus lag are
836 represented on the abscissa and ordinate and the color axis represents the strength of the
837 correlation. The *raw* eq-jpsth was first computed and then, the trials were shuffled for one variable
838 and the same matrix was obtained, the *shuffled* eq-jpsth. This procedure was performed 100 times to
839 obtain a distribution of 100 *shuffled* matrices. The corrected matrix was obtained by subtracting the
840 mean of the 100 *shuffled* matrices from the *raw* matrix and to divide this *subtracted* matrix by the
841 square root of the cross product of the time-dependent variance of the *raw* matrix. The scale of the
842 *subtracted* eq-jpsth is thereby bounded between -1 and 1 and named correlation coefficients. At
843 each point in the *subtracted* eq-jpsth, a correlation was considered significant if the value in that
844 point in the *raw* matrix (before correction) was always superior or always inferior to the 100 values

845 from the *shuffle* matrices in the same point (Fig. 6C-E). The data along the diagonal and paradiagonal
846 of the *subtracted* matrix were averaged to obtain cross correlograms (Fig. 6F-H). The lag with the
847 largest negative value (anticorrelation) was determined in the trial period prior to and after valid SC
848 onset.
849

AUTHOR CONTRIBUTIONS

SN: Conceptualization, Software, Formal analysis, Writing - Original Draft. **LLG**: Software, Formal analysis, Writing - Review & Editing. **EC**: Formal analysis, Writing - Review & Editing. **JP**: Investigation, Writing - Review & Editing. **FVB**: Software, Supervision, Writing - Review & Editing. **BEK**: Conceptualization, Software, Data Curation, Investigation, Supervision, Writing - Original Draft, Funding acquisition.

DECLARATION OF INTERESTS

The authors declare no competing interests.

ACKNOWLEDGEMENTS

The authors wish to thank Joel Baurberg, Xavier Degiovanni and Luc Renaud for technical assistance, Sébastien Barniaud, Laurence Boes, Frédéric Charlin and Marc Martin for animal care.

FUNDING

This work was supported by funding from the H2020-MSCA-ITN grant *In2PrimateBrains* (#956669) and the FLAG-ERA grant *PrimCorNet*, by ANR (ANR-19-HBPR-0005) to BEK.

REFERENCES

1. Jasper, H., and Penfield, W. (1949). Electrocorticograms in man: Effect of voluntary movement upon the electrical activity of the precentral gyrus. Arch. F. Psychiatr. U. Z. Neur. *183*, 163–174. 10.1007/BF01062488.

2. Salmelin, R., Hämäläinen, M., Kajola, M., and Hari, R. (1995). Functional segregation of movement-related rhytmic activity in the human brain. NeuroImage, 237–243.

3. Conway, B.A., Halliday, D.M., Farmer, S.F., Shahani, U., Maas, P., Weir, A.I., and Rosenberg, J.R. (1995). Synchronization between motor cortex and spinal motoneuronal pool during the performance of a maintained motor task in man. The Journal of Physiology *489*, 917–924. 10.1113/jphysiol.1995.sp021104.

4. Baker, S.N., Kilner, J.M., Pinches, E.M., and Lemon, R.N. (1999). The role of synchrony and oscillations in the motor output. Experimental Brain Research *128*, 109–117. 10.1007/s002210050825.

5. Brown, P. (2000). Cortical drives to human muscle: the Piper and related rhythms. Progress in Neurobiology *60*, 97–108. 10.1016/S0301-0082(99)00029-5.

6. Engel, A.K., and Fries, P. (2010). Beta-band oscillations — signalling the status quo? Current Opinion in Neurobiology *20*, 156–165. 10.1016/j.conb.2010.02.015.

7. van Ede, F., Jensen, O., and Maris, E. (2010). Tactile expectation modulates pre-stimulus β-band oscillations in human sensorimotor cortex. NeuroImage *51*, 867–876. 10.1016/j.neuroimage.2010.02.053.

8. van Ede, F., de Lange, F., Jensen, O., and Maris, E. (2011). Orienting Attention to an Upcoming Tactile Event Involves a Spatially and Temporally Specific Modulation of Sensorimotor Alpha- and Beta-Band Oscillations. J. Neurosci. *31*, 2016–2024. 10.1523/JNEUROSCI.5630-10.2011.

9. Jenkinson, N., and Brown, P. (2011). New insights into the relationship between dopamine, beta oscillations and motor function. Trends in Neurosciences *34*, 611–618. 10.1016/j.tins.2011.09.003.

10. Khanna, P., and Carmena, J.M. (2015). Neural oscillations: beta band activity across motor networks. Current Opinion in Neurobiology *32*, 60–67. 10.1016/j.conb.2014.11.010.

11. Peles, O., Werner-Reiss, U., Bergman, H., Israel, Z., and Vaadia, E. (2020). Phase-Specific Microstimulation Differentially Modulates Beta Oscillations and Affects Behavior. Cell Reports *30*, 2555-2566.e3. 10.1016/j.celrep.2020.02.005.

12. Murthy, V.N., and Fetz, E.E. (1992). Coherent 25- to 35-Hz oscillations in the sensorimotor cortex of awake behaving monkeys. Proc. Natl. Acad. Sci. U.S.A. *89*, 5670–5674. 10.1073/pnas.89.12.5670.

13. Murthy, V.N., and Fetz, E.E. (1996). Synchronization of neurons during local field potential oscillations in sensorimotor cortex of awake monkeys. Journal of Neurophysiology *76*, 3968–3982. 10.1152/jn.1996.76.6.3968.

14. Sanes, J.N., and Donoghue, J.P. (1993). Oscillations in local field potentials of the primate motor cortex during voluntary movement. Proc. Natl. Acad. Sci. U.S.A. *90*, 4470–4474. 10.1073/pnas.90.10.4470.

15. Rubino, D., Robbins, K.A., and Hatsopoulos, N.G. (2006). Propagating waves mediate information transfer in the motor cortex. Nat Neurosci *9*, 1549–1557. 10.1038/nn1802.

16. Androulidakis, A.G., Doyle, L.M.F., Gilbertson, T.P., and Brown, P. (2006). Corrective movements in response to displacements in visual feedback are more effective during periods of 13-35 Hz oscillatory synchrony in the human corticospinal system. European Journal of Neuroscience *24*, 3299–3304. 10.1111/j.1460-9568.2006.05201.x.

17. Lalo, E., Gilbertson, T., Doyle, L., Lazzaro, V.D., Cioni, B., and Brown, P. (2007). Phasic increases in cortical beta activity are associated with alterations in sensory processing in the human. Exp Brain Res *177*, 137–145. 10.1007/s00221-006-0655-8.

18. Saleh, M., Reimer, J., Penn, R., Ojakangas, C.L., and Hatsopoulos, N.G. (2010). Fast and Slow Oscillations in Human Primary Motor Cortex Predict Oncoming Behaviorally Relevant Cues. Neuron *65*, 461–471. 10.1016/j.neuron.2010.02.001.

19. Fujioka, T., Trainor, L.J., Large, E.W., and Ross, B. (2012). Internalized Timing of Isochronous Sounds Is Represented in Neuromagnetic Beta Oscillations. J. Neurosci. *32*, 1791–1802. 10.1523/JNEUROSCI.4107-11.2012.

20. Kilavik, B.E., Confais, J., and Riehle, A. (2014). Signs of Timing in Motor Cortex During Movement Preparation and Cue Anticipation. In Neurobiology of Interval Timing Advances in Experimental Medicine and Biology., H. Merchant and V. de Lafuente, eds. (Springer New York), pp. 121–142. 10.1007/978-1-4939-1782-2_7.

21. Wiener, M., Parikh, A., Krakow, A., and Coslett, H.B. (2018). An Intrinsic Role of Beta Oscillations in Memory for Time Estimation. Sci Rep *8*, 7992. 10.1038/s41598-018-26385-6.

22. Sun, H., Ma, X., Tang, L., Han, J., Zhao, Y., Xu, X., Wang, L., Zhang, P., Chen, L., Zhou, J., et al. (2019). Modulation of Beta Oscillations for Implicit Motor Timing in Primate Sensorimotor Cortex during Movement Preparation. Neurosci. Bull. *35*, 826–840. 10.1007/s12264-019-00387-4.

23. Kilavik, B.E., Zaepffel, M., Brovelli, A., MacKay, W.A., and Riehle, A. (2013). The ups and downs of beta oscillations in sensorimotor cortex. Experimental Neurology *245*, 15–26. 10.1016/j.expneurol.2012.09.014.

24. Spitzer, B., and Haegens, S. (2017). Beyond the Status Quo: A Role for Beta Oscillations in Endogenous Content (Re)Activation. eNeuro *4*, ENEURO.0170-17.2017. 10.1523/ENEURO.0170-17.2017.

25. Schmidt, R., Herrojo Ruiz, M., Kilavik, B.E., Lundqvist, M., Starr, P.A., and Aron, A.R. (2019). Beta Oscillations in Working Memory, Executive Control of Movement and Thought, and Sensorimotor Function. J. Neurosci. *39*, 8231–8238. 10.1523/JNEUROSCI.1163-19.2019.

26. Barone, J., and Rossiter, H.E. (2021). Understanding the Role of Sensorimotor Beta Oscillations. Front. Syst. Neurosci. *15*, 655886. 10.3389/fnsys.2021.655886.

27. Kilavik, B.E., Ponce-Alvarez, A., Trachel, R., Confais, J., Takerkart, S., and Riehle, A. (2012). Context-Related Frequency Modulations of Macaque Motor Cortical LFP Beta Oscillations. Cerebral Cortex *22*, 2148–2159. 10.1093/cercor/bhr299.

28. Confais, J., Malfait, N., Brochier, T., Riehle, A., and Kilavik, B.E. (2020). Is there an Intrinsic Relationship between LFP Beta Oscillation Amplitude and Firing Rate of Individual Neurons in Macaque Motor Cortex? Cerebral Cortex Communications *1*, tgaa017. 10.1093/texcom/tgaa017.

29. Stoll, F.M., Wilson, C.R.E., Faraut, M.C.M., Vezoli, J., Knoblauch, K., and Procyk, E. (2016). The Effects of Cognitive Control and Time on Frontal Beta Oscillations. Cereb. Cortex *26*, 1715–1732. 10.1093/cercor/bhv006.

30. Chandrasekaran, C., Bray, I.E., and Shenoy, K.V. (2019). Frequency Shifts and Depth Dependence of Premotor Beta Band Activity during Perceptual Decision-Making. J. Neurosci. *39*, 1420–1435. 10.1523/JNEUROSCI.1066-18.2018.

31. Zhang, Y., Wang, X., Bressler, S.L., Chen, Y., and Ding, M. (2008). Prestimulus Cortical Activity is Correlated with Speed of Visuomotor Processing. Journal of Cognitive Neuroscience *20*, 1915–1925. 10.1162/jocn.2008.20132.

32. Musall, S., Kaufman, M.T., Juavinett, A.L., Gluf, S., and Churchland, A.K. (2019). Single-trial neural dynamics are dominated by richly varied movements. Nat Neurosci *22*, 1677–1686. 10.1038/s41593-019-0502-4.

33. Tremblay, S., Testard, C., DiTullio, R.W., Inchauspé, J., and Petrides, M. (2023). Neural cognitive signals during spontaneous movements in the macaque. Nat Neurosci *26*, 295–305. 10.1038/s41593-022-01220-4.

34. Kühn, A.A., Fogelson, N., Limousin, P.D., Hariz, M.I., Kupsch, A., and Brown, P. (2009). Frequency-specific effects of stimulation of the subthalamic area in treated Parkinson's disease patients. NeuroReport *20*, 975–978. 10.1097/WNR.0b013e32832d2456.

35. Neumann, W.-J., Degen, K., Schneider, G.-H., Brücke, C., Huebl, J., Brown, P., and Kühn, A.A. (2016). Subthalamic synchronized oscillatory activity correlates with motor impairment in patients with Parkinson's disease: Correlation of Subthalamic B Oscillations and PD Symptoms. Mov Disord. *31*, 1748–1751. 10.1002/mds.26759.

36. López-Azcárate, J., Tainta, M., Rodríguez-Oroz, M.C., Valencia, M., González, R., Guridi, J., Iriarte, J., Obeso, J.A., Artieda, J., and Alegre, M. (2010). Coupling between Beta and High-Frequency Activity in the Human Subthalamic Nucleus May Be a Pathophysiological Mechanism in Parkinson's Disease. J. Neurosci. *30*, 6667–6677. 10.1523/JNEUROSCI.5459-09.2010.

37. Priori, A., Foffani, G., Pesenti, A., Tamma, F., Bianchi, A., Pellegrini, M., Locatelli, M., Moxon, K., and Villani, R. (2004). Rhythm-specific pharmacological modulation of subthalamic activity in Parkinson's disease. Experimental Neurology *189*, 369–379. 10.1016/j.expneurol.2004.06.001.

38. Schwey A, Battaglia D, Bahuguna J, Malfait N (2023). Different faces of medial beta-band activity reflect distinct visuomotor feedback signals. J Neurosci (in press). The Journal of Neuroscience.

39. Lundqvist, M., Rose, J., Herman, P., Brincat, S.L., Buschman, T.J., and Miller, E.K. (2016). Gamma and Beta Bursts Underlie Working Memory. Neuron *90*, 152–164. 10.1016/j.neuron.2016.02.028.

40. Haegens, S., Vergara, J., Rossi-Pool, R., Lemus, L., and Romo, R. (2017). Beta oscillations reflect supramodal information during perceptual judgment. Proc. Natl. Acad. Sci. U.S.A. *114*, 13810–13815. 10.1073/pnas.1714633115.

41. Vezoli, J., Vinck, M., Bosman, C.A., Bastos, A.M., Lewis, C.M., Kennedy, H., and Fries, P. (2021). Brain rhythms define distinct interaction networks with differential dependence on anatomy. Neuron *109*, 3862-3878.e5. 10.1016/j.neuron.2021.09.052.

42. Pershin, I., Candrian, G., Münger, M., Baschera, G.-M., Rostami, M., Eich, D., and Müller, A. (2023). Vigilance described by the time-on-task effect in EEG activity during a cued Go/NoGo task. International Journal of Psychophysiology *183*, 92–102. 10.1016/j.ijpsycho.2022.11.015.

43. Hafed, Z.M., and Clark, J.J. (2002). Microsaccades as an overt measure of covert attention shifts. Vision Research *42*, 2533–2545. 10.1016/S0042-6989(02)00263-8.

44. Ortega, J., Plaska, C.R., Gomes, B.A., and Ellmore, T.M. (2022). Spontaneous Eye Blink Rate During the Working Memory Delay Period Predicts Task Accuracy. Front. Psychol. *13*, 788231. 10.3389/fpsyg.2022.788231.

45. Donoghue, J.P., Sanes, J.N., Hatsopoulos, N.G., and Gaál, G. (1998). Neural Discharge and Local Field Potential Oscillations in Primate Motor Cortex During Voluntary Movements. Journal of Neurophysiology *79*, 159–173. 10.1152/jn.1998.79.1.159.

46. Feingold, J., Gibson, D.J., DePasquale, B., and Graybiel, A.M. (2015). Bursts of beta oscillation differentiate postperformance activity in the striatum and motor cortex of monkeys performing movement tasks. Proc. Natl. Acad. Sci. U.S.A. *112*, 13687–13692. 10.1073/pnas.1517629112.

47. Rougeul, A., Bouyer, J.J., Dedet, L., and Debray, O. (1979). Fast somato-parietal rhythms during combined focal attention and immobility in baboon and squirrel monkey. Electroencephalography and Clinical Neurophysiology *46*, 310–319. 10.1016/0013-4694(79)90205-0.

48. Courtemanche, R., and Lamarre, Y. (2005). Local Field Potential Oscillations in Primate Cerebellar Cortex: Synchronization With Cerebral Cortex During Active and Passive Expectancy. Journal of Neurophysiology *93*, 2039–2052. 10.1152/jn.00080.2004.

49. Witham, C.L., and Baker, S.N. (2007). Network oscillations and intrinsic spiking rhythmicity do not covary in monkey sensorimotor areas: Oscillations and rhythmic firing. The Journal of Physiology *580*, 801–814. 10.1113/jphysiol.2006.124503.

50. Witham, C.L., Wang, M., and Baker, S.N. (2007). Cells in somatosensory areas show synchrony with beta oscillations in monkey motor cortex: Oscillatory synchrony in somatosensory areas. European Journal of Neuroscience *26*, 2677–2686. 10.1111/j.1460-9568.2007.05890.x.

51. Haegens, S., Nácher, V., Hernández, A., Luna, R., Jensen, O., and Romo, R. (2011). Beta oscillations in the monkey sensorimotor network reflect somatosensory decision making. Proc. Natl. Acad. Sci. U.S.A. *108*, 10708–10713. 10.1073/pnas.1107297108.

52. Zanos, S., Rembado, I., Chen, D., and Fetz, E.E. (2018). Phase-Locked Stimulation during Cortical Beta Oscillations Produces Bidirectional Synaptic Plasticity in Awake Monkeys. Current Biology *28*, 2515-2526.e4. 10.1016/j.cub.2018.07.009.

53. Buschman, T.J., and Miller, E.K. (2007). Top-Down Versus Bottom-Up Control of Attention in the Prefrontal and Posterior Parietal Cortices. Science *315*, 1860–1862. 10.1126/science.1138071.

54. Buschman, T.J., Denovellis, E.L., Diogo, C., Bullock, D., and Miller, E.K. (2012). Synchronous Oscillatory Neural Ensembles for Rules in the Prefrontal Cortex. Neuron *76*, 838–846. 10.1016/j.neuron.2012.09.029.

55. Rassi, E., Zhang, Y., Mendoza, G., Méndez, J.C., Merchant, H., and Haegens, S. (2023). Distinct beta frequencies reflect categorical decisions. Nat Commun *14*, 2923. 10.1038/s41467-023-38675-3.

56. Rosanova, M., Casali, A., Bellina, V., Resta, F., Mariotti, M., and Massimini, M. (2009). Natural Frequencies of Human Corticothalamic Circuits. Journal of Neuroscience *29*, 7679–7685. 10.1523/JNEUROSCI.0445-09.2009.

57. Mahjoory, K., Schoffelen, J.-M., Keitel, A., and Gross, J. (2020). The frequency gradient of human resting-state brain oscillations follows cortical hierarchies. eLife *9*, e53715. 10.7554/eLife.53715.

58. Courtemanche, R., Fujii, N., and Graybiel, A.M. Synchronous, Focally Modulated ᴺᴸ-Band Oscillations Characterize Local Field Potential Activity in the Striatum of Awake Behaving Monkeys.

59. Echeverria-Altuna, I., Quinn, A.J., Zokaei, N., Woolrich, M.W., Nobre, A.C., and van Ede, F. (2022). Transient beta activity and cortico-muscular connectivity during sustained motor behaviour. Progress in Neurobiology *214*, 102281. 10.1016/j.pneurobio.2022.102281.

60. Witham, C.L., Wang, M., and Baker, S.N. (2010). Corticomuscular coherence between motor cortex, somatosensory areas and forearm muscles in the monkey. Front. Syst. Neurosci. 10.3389/fnsys.2010.00038.

61. Witham, C.L., Riddle, C.N., Baker, M.R., and Baker, S.N. (2011). Contributions of descending and ascending pathways to corticomuscular coherence in humans: Descending and ascending corticomuscular coherence. The Journal of Physiology *589*, 3789–3800. 10.1113/jphysiol.2011.211045.

62. Jensen, O., Goel, P., Kopell, N., Pohja, M., Hari, R., and Ermentrout, B. (2005). On the human sensorimotor-cortex beta rhythm: Sources and modeling. NeuroImage *26*, 347–355. 10.1016/j.neuroimage.2005.02.008.

63. Lundqvist, M., Bastos, A.M., and Miller, E.K. (2020). Preservation and Changes in Oscillatory Dynamics across the Cortical Hierarchy. Journal of Cognitive Neuroscience *32*, 2024–2035. 10.1162/jocn_a_01600.

64. Chota, S., VanRullen, R., and Gulbinaite, R. (2023). Random Tactile Noise Stimulation Reveals Beta-Rhythmic Impulse Response Function of the Somatosensory System. J. Neurosci. *43*, 3107–3119. 10.1523/JNEUROSCI.1758-22.2023.

65. Vinck, M., Uran, C., Spyropoulos, G., Onorato, I., Broggini, A.C., Schneider, M., and Canales-Johnson, A. (2023). Principles of large-scale neural interactions. Neuron *111*, 987–1002. 10.1016/j.neuron.2023.03.015.

66. Kilavik, B.E., Confais, J., Ponce-Alvarez, A., Diesmann, M., and Riehle, A. (2010). Evoked Potentials in Motor Cortical Local Field Potentials Reflect Task Timing and Behavioral Performance. Journal of Neurophysiology *104*, 2338–2351. 10.1152/jn.00250.2010.

67. Ponce-Alvarez, A., Kilavik, B.E., and Riehle, A. (2010). Comparison of local measures of spike time irregularity and relating variability to firing rate in motor cortical neurons. J Comput Neurosci *29*, 351–365. 10.1007/s10827-009-0158-2.

68. Confais, J., Kilavik, B.E., Ponce-Alvarez, A., and Riehle, A. (2012). On the Anticipatory Precue Activity in Motor Cortex. J. Neurosci. *32*, 15359–15368. 10.1523/JNEUROSCI.1768-12.2012.

69. Asanuma, H., and Rosén, I. (1972). Topographical organization of cortical efferent zones projecting to distal forelimb muscles in the monkey. Exp Brain Res *14*, 243–256. 10.1007/BF00816161.

70. de Haan, M.J., Brochier, T., Grün, S., Riehle, A., and Barthélemy, F.V. (2018). Real-time visuomotor behavior and electrophysiology recording setup for use with humans and monkeys. Journal of Neurophysiology *120*, 539–552. 10.1152/jn.00262.2017.

71. Crameri, F. (2019). Scientific Colour Maps (Zenodo) 10.5281/ZENODO.3596401.

72. Donoghue, T., Haller, M., Peterson, E.J., Varma, P., Sebastian, P., Gao, R., Noto, T., Lara, A.H., Wallis, J.D., Knight, R.T., et al. (2020). Parameterizing neural power spectra into periodic and aperiodic components. Nat Neurosci *23*, 1655–1665. 10.1038/s41593-020-00744-x.

73. Berens, P. (2009). CircStat: A MATLAB Toolbox for Circular Statistics. J. Stat. Soft. *31*. 10.18637/jss.v031.i10.

74. Pedregosa, F., Varoquaux, G., Gramfort, A., Michel, V., Thirion, B., Grisel, O., Blondel, M., Prettenhofer, P., Weiss, R., Dubourg, V., et al. Scikit-learn: Machine Learning in Python. MACHINE LEARNING IN PYTHON.

75. Aertsen, A.M., Gerstein, G.L., Habib, M.K., and Palm, G. (1989). Dynamics of neuronal firing correlation: modulation of “effective connectivity.” Journal of Neurophysiology *61*, 900–917. 10.1152/jn.1989.61.5.900.

76. Nougaret, S., and Genovesio, A. (2018). Learning the meaning of new stimuli increases the cross-correlated activity of prefrontal neurons. Sci Rep *8*, 11680. 10.1038/s41598-018-29862-0.

77. Oostenveld, R., Fries, P., Maris, E., and Schoffelen, J.-M. (2011). FieldTrip: Open Source Software for Advanced Analysis of MEG, EEG, and Invasive Electrophysiological Data. Computational Intelligence and Neuroscience *2011*, 1–9. 10.1155/2011/156869.

1095 **FIGURE LEGENDS**

1096 **Figure 1. Experimental setup and task, spontaneous hand and eye movements.**

1097 A. The monkeys were seated in a primate chair, and performed center-out arm reaching
1098 responses with a manipulandum in the horizontal plane, with the visual scene displayed on a vertical
1099 monitor. Eye position was recorded using an infrared camera.

1100 B. The monkeys performed a visuomotor delayed match to sample task with fixed cue order and a
1101 GO signal. The trial started when the monkey moved the hand cursor to the central fixation spot
1102 (touch). Next, a selection cue (SEL) indicated the color to attend in that trial (sample). Thereafter
1103 three spatial cues (SC) were presented in sequence in fixed order (blue SC1 – green SC2 – pink SC3),
1104 each in one of the four possible peripheral target positions. A directionally non-informative GO signal
1105 indicated to the monkey to initiate the center-out reaching movement to the memorized valid
1106 (match) target location. Each delay lasted 1s and each visual cue lasted 300ms.

1107 C. Average hand velocity across all trials in all behavioral sessions for each monkey, zoomed in to
1108 the micro-movements performed during the trial between central touch and the GO signal. In this
1109 and subsequent figures, the blue, green and pink lines reflect data split according to the color
1110 condition and vertical lines reflect onset/offset of task events.

1111 D. Average eye velocity for each monkey across all trials in all behavioral sessions with eye
1112 movement recordings. Same conventions as in C.

1113 E. Gaze position for monkey T, across all trials in all behavioral sessions with eye movement
1114 recordings, in blue (upper), green (middle) and pink (bottom) color conditions. Each plot show the
1115 proportion of trials with eye gaze on the Target SC (cyan), on one of the other peripheral target
1116 outlines (orange), on the central fixation spot (yellow), between different visual items but within the
1117 work area (purple), outside the work area (i.e. outside the monitor; gray) or eyeblinks (black).

1118 F. Gaze position for Monkey M. Same conventions as in E.

1119

1120 **Figure 2. Example LFP sites and grand average spectrograms.**

1121 A-C. Spectrograms of three simultaneously recorded LFP sites from monkey T, including all correct
1122 trials in one session, separated for the blue (top), green (middle) and pink (bottom) color conditions.
1123 The locations of the three example LFP sites are marked with stars in Figure 3C, with site 1 more
1124 anterior and site 3 more posterior. Frequency is on the vertical axis and task events are indicated
1125 along the horizontal axis (vertical white lines). Warmer colors indicate increased power (a.u.).

1126 D. Single trial examples of LFPs filtered broadly around the beta frequency range (8-45Hz), for LFP
1127 site 1. Five trials per color condition are shown.

1128 E. Grand average spectrograms for each monkey, including normalized individual trials for all LFP
1129 sites in each monkey.

1130 F. As in D, but for LFP site 3.

1131

1132 **Figure 3. Concurrent low and high beta band rhythms in the motor cortex.**

1133 A. Average normalized power spectra in the pre-SC1 period across all trials for all sites in each
1134 monkey, after removing the aperiodic signal component. The curves reflect the mean power ±SEM
1135 across LFP sites. Overlain are distributions of single-trial peak frequency (frequency with maximal
1136 power) between 10-40Hz in the same task period, in the periodic-only signal component.

1137 B. Distribution of the beta band dominance index for all LFP sites for each monkey, based on the
1138 periodic-only signal component in the pre-SC1 period. Positive indices reflect low band (13-19Hz)
1139 dominance and negative indices reflect high band (23-29Hz) dominance. Light gray bars include all
1140 sites, and dark gray bars sites with significantly different power in the low and high beta frequency
1141 ranges (paired t-test, $p<0.05$).

1142 C. Beta band dominance indices plotted as a function of LFP site coordinates on the cortical
1143 surface. The indices for both monkeys are plotted on top of the MRI-based cortical surface
1144 reconstruction of monkey T (anterior towards the left, and medial towards the top). Blue sites reflect
1145 high band dominance, and yellow sites low band dominance. The three sites from anterior to

posterior marked with red stars reflect the example sites shown in Fig. 2. CS central sulcus; AS arcuate sulcus; PCD precentral dimple.

Figure 4. Average low and high beta amplitude, and main regressors explaining amplitude variance.

A. Representation of the trial-averaged temporal profile of normalized high (left ; 21-29Hz) and low (right ; 12-20Hz) beta amplitude (+/-SEM), separated by the 3 color conditions. The horizontal gray line above each plot graph represents the time-resolved modulation in beta amplitude by the color condition. The significativity is represented as a gray-scale gradient (brightest gray for p=0.01 and darkest gray for p<=1e-08; white means non-significant)..

B. Time-resolved representation of the presence of each regressor in the winning model after the application of a Bayesian Index Criterion (BIC) for the comparison of all possible models and their 2-by-2 interactions, for the high beta (left) and the low beta (right). Each row represents a regressor, the last row represents all possible interactions. Regressors selected for ulterior analysis in orange and discarded regressors in gray.

C. Significativity of the correlation between high (left) and low (right) beta and hand velocity, for each color condition separately. For each condition, positive correlations are represented at the top and negative at the bottom. The same gradient of brightness as in B was applied to represent the significativity. In all plots, n represents the number of included trials in the analysis.

Figure 5. Beta amplitude modulations in error trials and trial condition decoding.

A. Trial-averaged beta amplitude in high beta (left) and low beta (right) in unambiguous correct and distractor error trials, split for the three color conditions from top to bottom. Only trials in which the target selected (correct or distractor) did not coincide in space with any of the two other SC are included. Thicker lines represent correct trials and thinner lines the error trials in which either one or the other distractor was used. Insets in the upper right corner show dimensionality reduction visualizations (t-SNE) for the unambiguous correct trials in the respective color conditions.

1173 B. Decoding performance of SEL (color condition) category in unambiguous correct trials, using
1174 either high (left) or low (right) beta band amplitude. Performance is presented as proportions of the
1175 total number of trials of each category in the test set (totalling 1 for each row). The diagonal
1176 represents the true positive accuracy, and the off-diagonal values correspond to the proportions of
1177 trials of each category incorrectly assigned to another category. The estimated chance level (0.37) is
1178 marked on the color scale bar.

1179 C. Decoding performance in distractor error trials, using the classifier previously trained on the
1180 unambiguous correct trials. The first column for each band represents the accuracy when predicting
1181 the attended distractor (i.e. what the monkey actually did); the second column represents the
1182 accuracy when predicting the correct SEL category (i.e. what the monkey should have done). The
1183 same chance level applies to these predictions as for the decoding of correct trials.

1184

1185 **Figure 6. Correlations of beta amplitude with RT and hand velocity.**

1186 A. High beta amplitude split into two groups based on normalized RT, for the quartiles of trials
1187 with longest (bright curves) and shortest (dark curves) RT in each session, for each color condition
1188 separately. Colored areas between the two curves indicate correlation significance (and sign)
1189 between high beta amplitude and RT, calculated across all trials. The hues of the shaded areas
1190 represent the sign of the significativity. Brighter hues represent positive correlations and darker hues
1191 negative correlations between beta amplitude and RT.

1192 B. Same representation for the low beta band.

1193 C-E. Left. Equivalent of a joint peristimulus time histogram applied to the hand velocity and the
1194 low beta amplitude along the trial. Each point of the matrix represents the corrected trial-by-trial
1195 cross product of the two variables. The analysis was performed separately for the 3 color conditions.
1196 Each colored matrix point was inferior (cold color) or superior (warm color) to 100 values from
1197 shuffled matrices (equivalent p-value of 0.01). The vertical and horizontal lines represent the
1198 appearance and disappearance of the valid SC for the 3 conditions. Gray shaded regions represent
1199 the trial periods considered in the corresponding cross-correlogram.

F-H. Cross correlograms for the three color conditions. Each value of the cross correlogram represents the average of main and para diagonals of the matrices, separately for before (bottom) and after (top) the onset of the valid SC. The circles on each curve represent the most negative value of the correlation. On the top plots (post-validSC), the vertical dash represents the moment of the most negative value in the pre-validSC period.

Figure 7. Correlation of high and low beta amplitude with gaze position.

A. High beta amplitude split in two groups based on gaze position, for each color condition. Dark curves for gaze In, and bright curves for gaze Out, in each time point for the beta amplitude considering the gaze position exactly 240ms before. The significativity is represented in the same way as in Figure 6A-B.

B. Same representation for the low beta band.

Figure 8. Increase in high and low beta amplitude with time-on-task.

A. High beta amplitude split in two groups based on time-on-task, for each color condition. Dark curves for the first third of trials and bright curves for the final third of trials in each session. The significativity is represented in the same way as in Figure 6A-B.

B. Same representation for the low beta band.

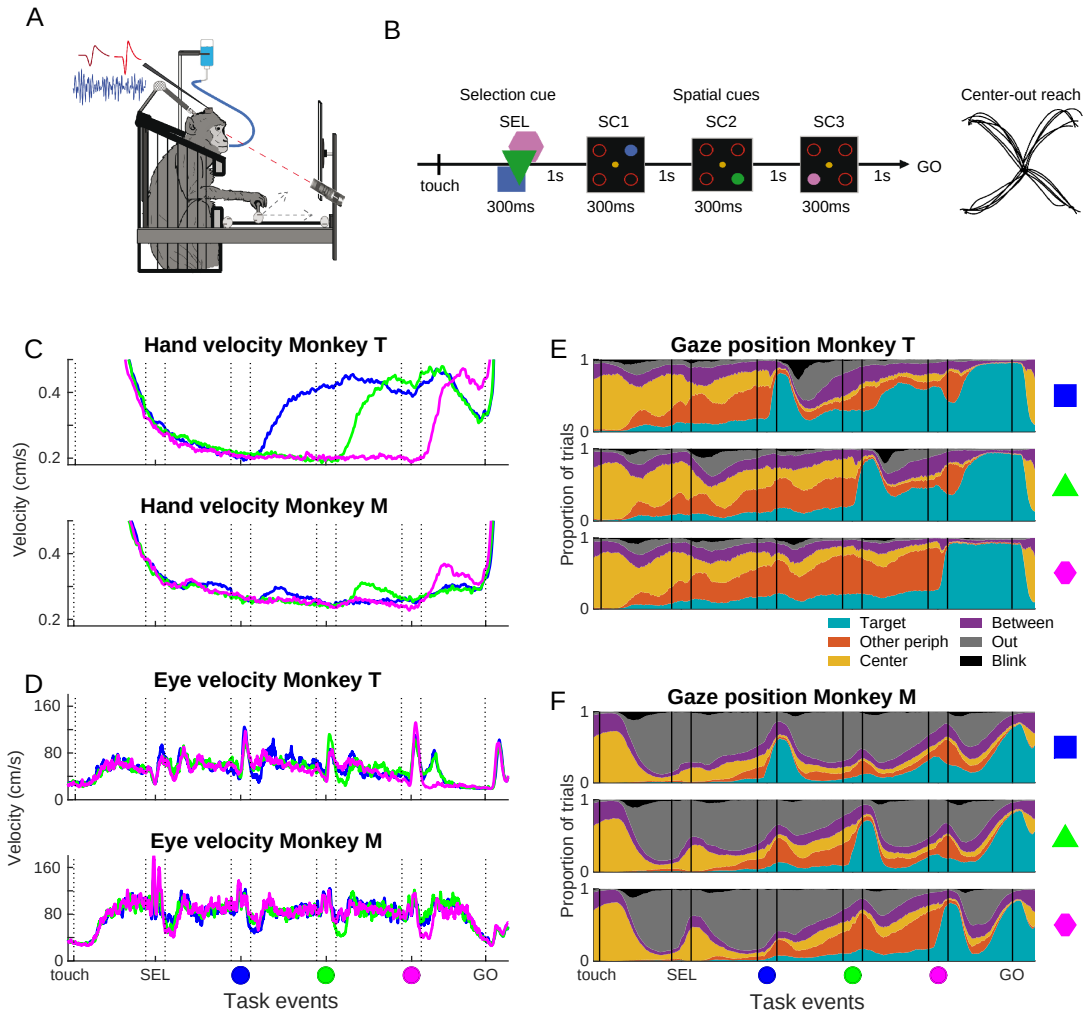
A
B
Selection cue
Spatial cues
Center-out reach
SEL
SC1
SC2
SC3
touch
1s
300ms
GO
C
Hand velocity Monkey T
Hand velocity Monkey M
Velocity (cm/s)
D
Eye velocity Monkey T
Eye velocity Monkey M
touch
SEL
GO
Task events
E
Gaze position Monkey T
Proportion of trials
Target
Other periph
Center
Between
Out
Blink
F
Gaze position Monkey M

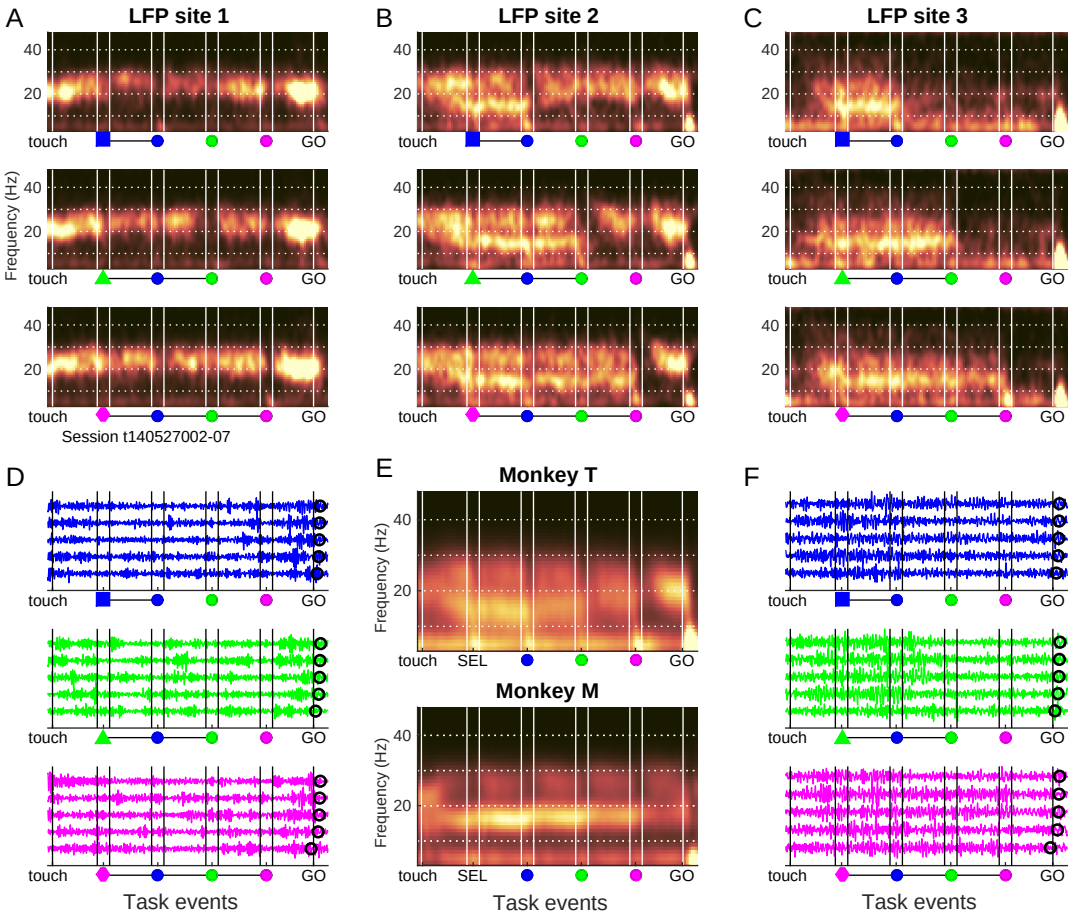
A
LFP site 1
B
LFP site 2
C
LFP site 3
40
20
touch
GO
Frequency (Hz)
Session t140527002-07
D
E
Monkey T
Monkey M
SEL
F
Task events

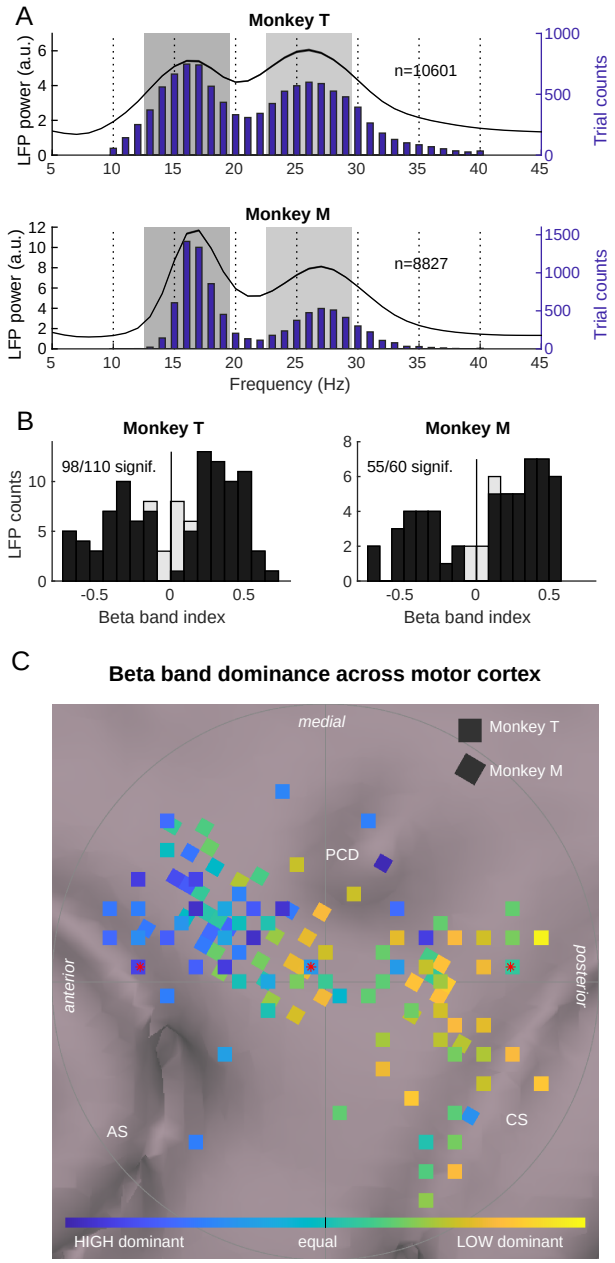
A
Monkey T
LFP power (a.u.)
Trial counts
n=10601
Monkey M
n=8827
Frequency (Hz)
B
Monkey T
98/110 signif.
LFP counts
Beta band index
Monkey M
55/60 signif.
C
Beta band dominance across motor cortex
medial
Monkey T
Monkey M
PCD
anterior
posterior
AS
CS
HIGH dominant
equal
LOW dominant

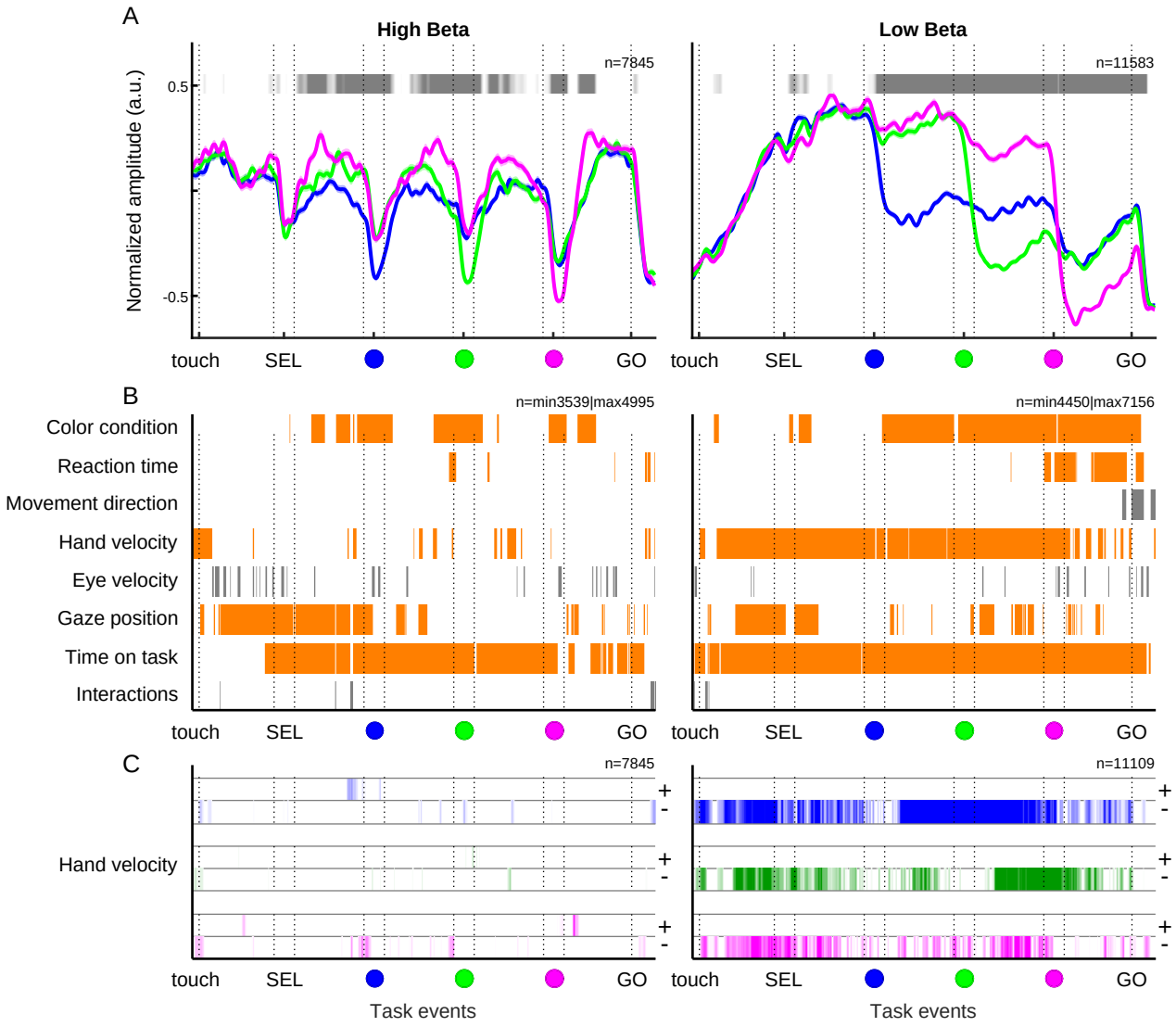
A
High Beta
Low Beta
n=7845
n=11583
Normalized amplitude (a.u.)
0.5
-0.5
touch
SEL
GO
B
n=min3539|max4995
n=min4450|max7156
Color condition
Reaction time
Movement direction
Hand velocity
Eye velocity
Gaze position
Time on task
Interactions
C
n=7845
n=11109
Hand velocity
+
-
Task events

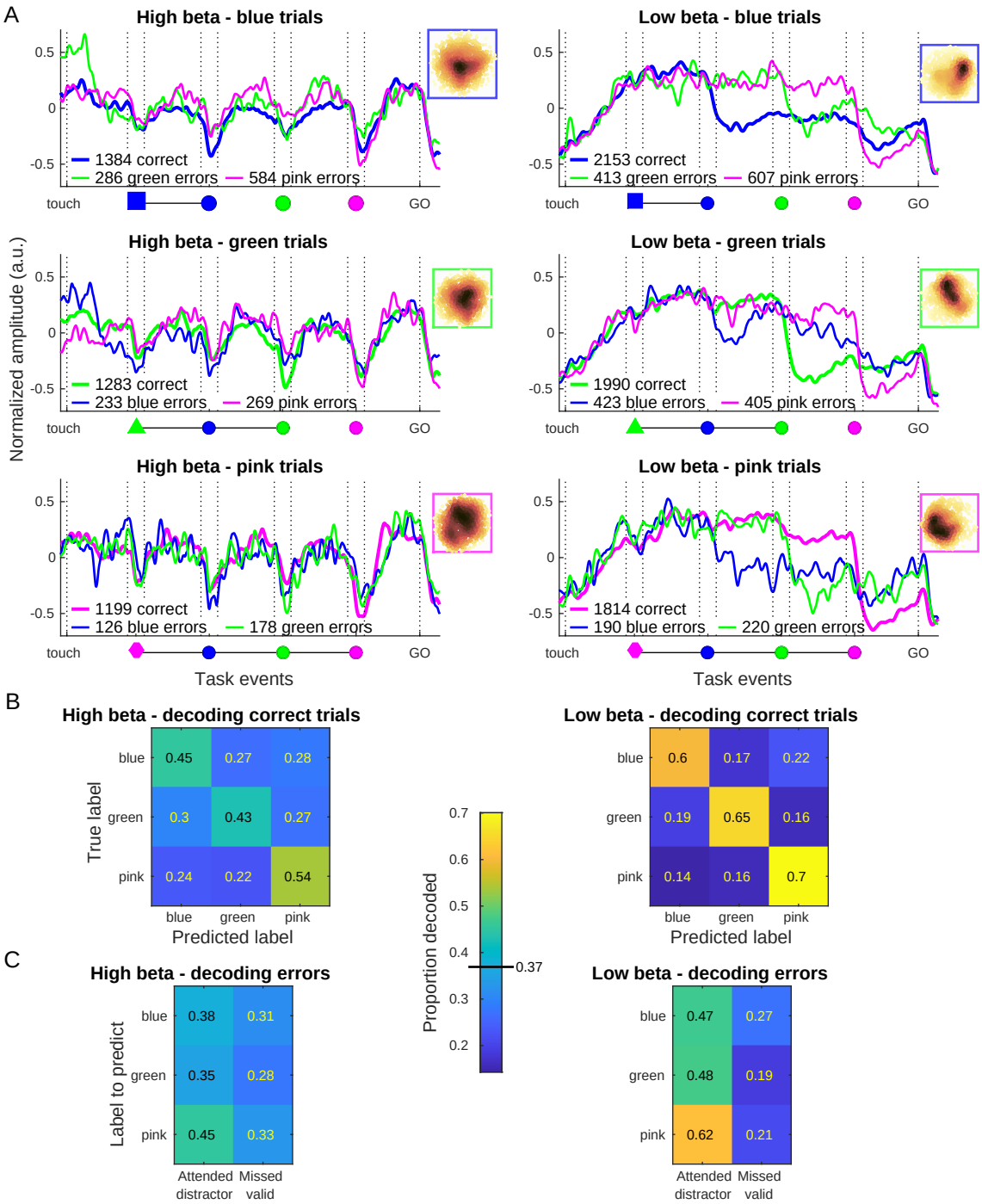
A
High beta - blue trials
1384 correct
286 green errors
584 pink errors
Low beta - blue trials
2153 correct
413 green errors
607 pink errors
High beta - green trials
1283 correct
233 blue errors
269 pink errors
Low beta - green trials
1990 correct
423 blue errors
405 pink errors
High beta - pink trials
1199 correct
126 blue errors
178 green errors
Low beta - pink trials
1814 correct
190 blue errors
220 green errors
touch
GO
Normalized amplitude (a.u.)
Task events
B
High beta - decoding correct trials
True label
Predicted label
blue 0.45 0.27 0.28
green 0.3 0.43 0.27
pink 0.24 0.22 0.54
Low beta - decoding correct trials
blue 0.6 0.17 0.22
green 0.19 0.65 0.16
pink 0.14 0.16 0.7
Proportion decoded
0.37
C
High beta - decoding errors
Label to predict
blue 0.38 0.31
green 0.35 0.28
pink 0.45 0.33
Attended distractor
Missed valid
Low beta - decoding errors
blue 0.47 0.27
green 0.48 0.19
pink 0.62 0.21

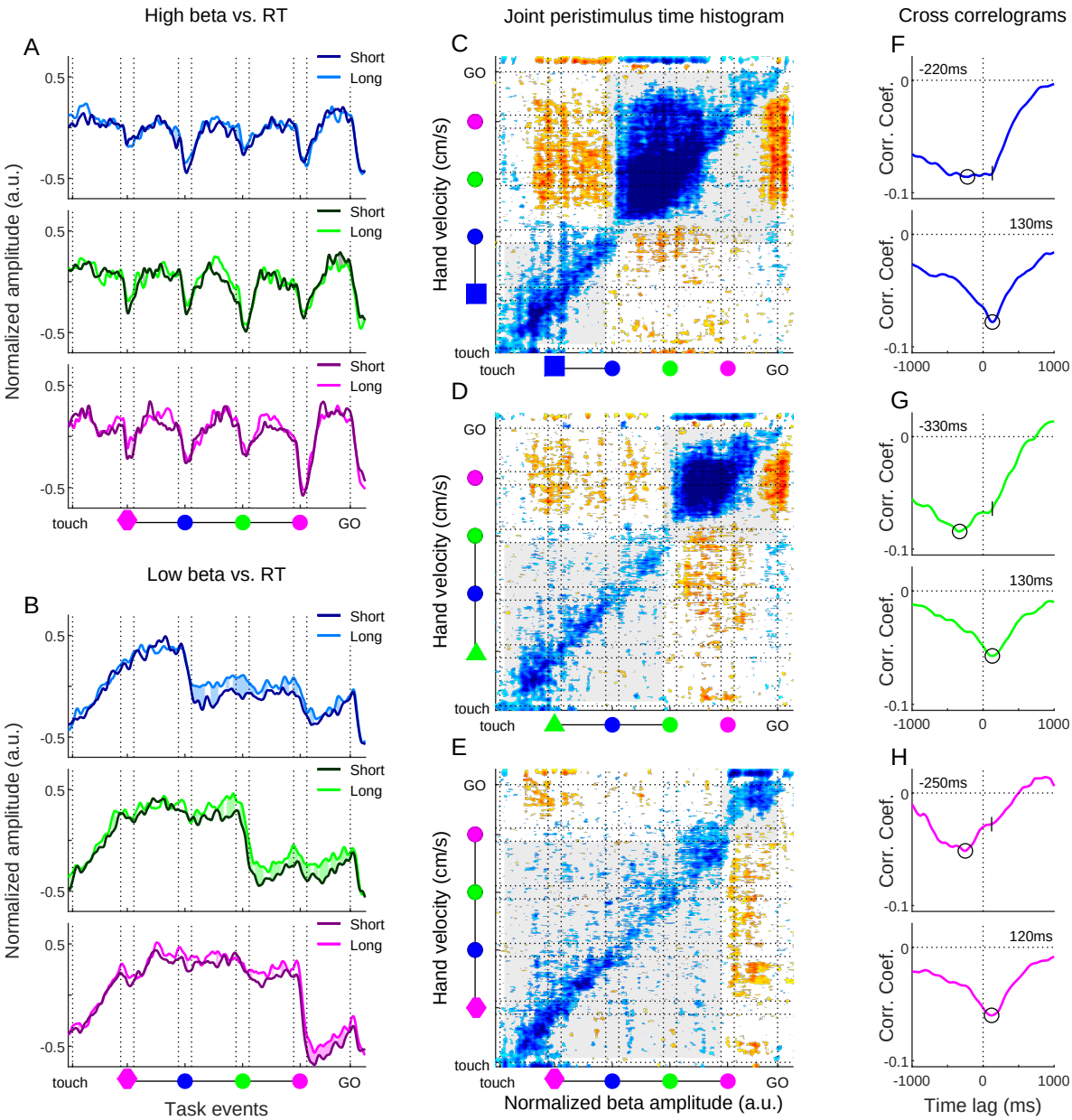
High beta vs. RT
Joint peristimulus time histogram
Cross correlograms
A
B
C
D
E
F
G
H
Short
Long
Normalized amplitude (a.u.)
Hand velocity (cm/s)
touch
GO
Low beta vs. RT
Task events
Normalized beta amplitude (a.u.)
Corr. Coef.
Time lag (ms)
-220ms
130ms
-330ms
130ms
-250ms
120ms

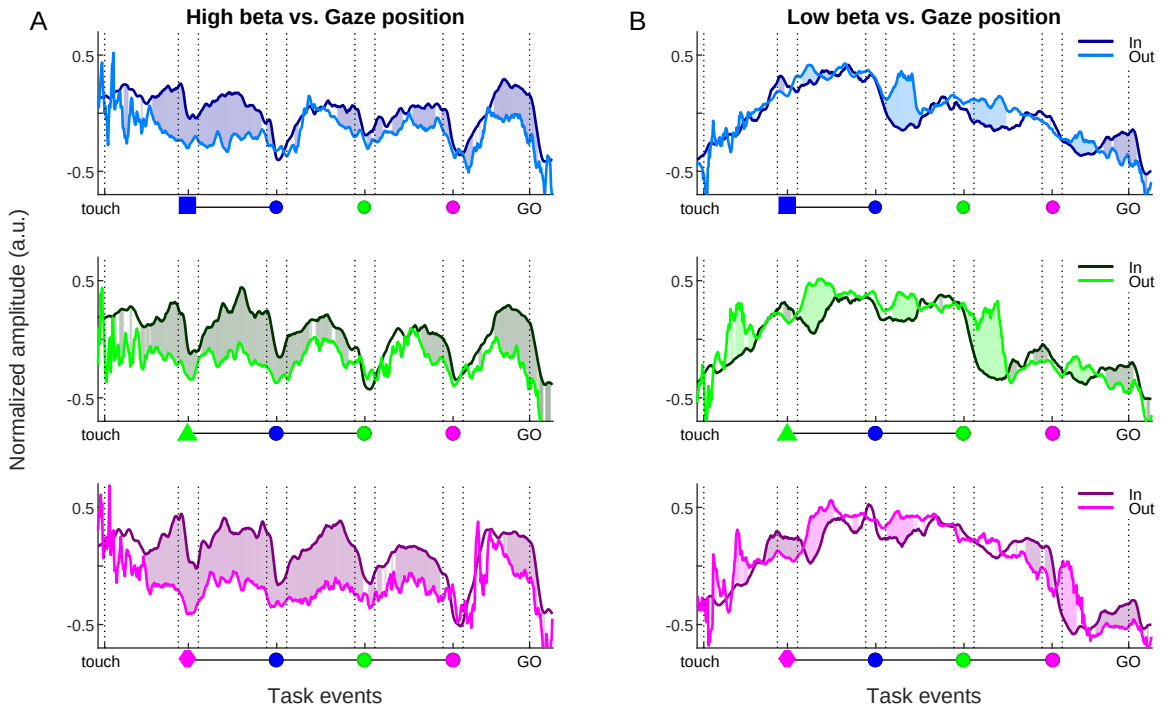
A
High beta vs. Gaze position
B
Low beta vs. Gaze position
Normalized amplitude (a.u.)
0.5
-0.5
touch
GO
In
Out
Task events

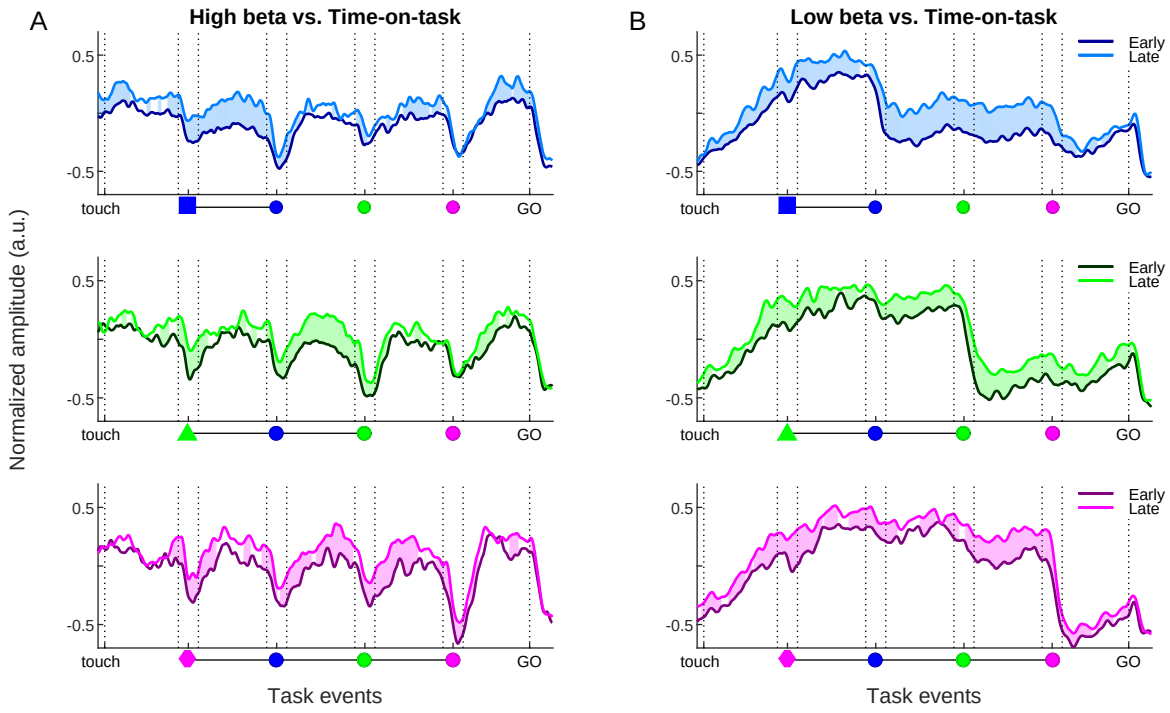
A
High beta vs. Time-on-task
B
Low beta vs. Time-on-task
Normalized amplitude (a.u.)
0.5
-0.5
touch
GO
Early
Late
Task events